Integral-equation methods for inhomogeneous elliptic partial differential equations in complex geometry

by

Travis Askham

A dissertation submitted in partial fulfillment

of the requirements for the degree of

Doctor of Philosophy

Department of Mathematics

Courant Institute of Mathematical Sciences

New York University

January 2016

_____

Leslie Greengard

Dedication

For Angie

Acknowledgements

I would first like to express my sincere gratitude to my advisor Leslie Greengard, who has been an inspiring collaborator and who has been generous with his time. I would also like to thank the rest of my committee, Antoine Cerfon, Michael O'Neil, Felipe Vico Bondía, and Michael Shelley, for their valuable notes and encouragement.

In addition to the collaborators on my committee, Manas Rachh and the rest of the Greengard research group have had a great impact on this work, through conversations over lunch, extended group meetings, and debugging assistance.

It is a wonderful thing to receive a piece of software from someone which does what it says it does, and in this I am thankful to Leslie Greengard, Michael O'Neil, Zydrunas Gimbutas, Manas Rachh, Antoine Cerfon, James Bremer, Kenneth Ho, and Sivaram Ambikasaran, among others.

The Courant Institute has been the perfect home for my graduate studies in mathematics and I am grateful to the faculty and staff for their role in this special place. The Graduate School of Arts and Sciences at New York University has been of great help as well and I am particularly appreciative of the dissertation fellowship which supported this work.

Finally, I would like to thank my friends and family for their support in these busy months; above all, I should thank my fiancée Angela Voyles, who kept my spirits up when the math got the better of me.

Abstract

Over the last several decades, integral-equation methods have emerged as powerful tools for the solution of the homogeneous partial differential equations of mathematical physics, including the Laplace, Helmholtz and Maxwell equations. By using the methods of potential theory, boundary value problems can be recast as boundary integral equations, reducing the dimensionality of the problem by one and permitting geometrically flexible discretization. Combined with suitable fast algorithms, this has led to optimal or nearly optimal complexity solvers in a variety of important application areas. For inhomogeneous, variable coefficient and nonlinear equations, there is no corresponding reduction in dimensionality, since the interior of the domain needs to be discretized and integral-equation methods appear to be less natural. They lead to dense linear systems of equations, while direct discretization of the partial differential equation leads to a sparse system of the same size.

In this thesis, we present a new collection of integral-equation methods for inhomogeneous partial differential equations including the Poisson, modified Helmholtz, and modified Stokes equations that are of optimal computational complexity, while fully adaptive, high order accurate and easy to use even in complex geometry. For this, we have combined fast methods for computing the volume integral operators of potential theory, with new quadrature methods for layer potentials, and a new method for smooth function extension from arbitrarily-shaped domains. Unlike finite difference and finite element discretization of the governing partial differential equation, the only unknowns in the formulation lie on the domain boundary, so that there is still an effective reduction in dimensionality in terms of the size of the linear system which needs to be solved. The interior degrees of freedom are

accounted for using an explicit integral transform, for which we have developed specialized versions of the fast multipole method. These tools can be extended in a straightforward manner to create fast, high order accurate solvers for more complex problems, including variable coefficient problems and the incompressible Navier-Stokes equations.

Contents

List of Figures

List of Tables

Introduction

The principal focus of this thesis is the development of numerical methods for elliptic partial differential equations (PDEs) that are both fast and accurate enough to permit design by simulation. Numerical methods in this regime should be capable of both solving the complex equations associated with engineering applications and meeting the requirements of design software — particularly when it comes to geometrically complex modeling, automatic adaptivity, and error estimation.

The target equations here are the Poisson, modified Hemlholtz and modified Stokes equations. Fast solvers for these equations are essential ingredients in solving more complex equations, such as the incompressible Navier-Stokes equations or a variety of nonlinear elliptic equations.

For the sake of illustration, suppose that we wish to solve the Poisson equation

$$-\Delta u(\mathbf{x}) = f(\mathbf{x}) \quad \text{in } \Omega \tag{1}$$

with Dirichlet boundary conditions

$$u(\mathbf{x}) = g(\mathbf{x}) \quad \text{on } \Gamma, \tag{2}$$

where Ω is a bounded domain in $\mathbb{R}^2$ with boundary Γ.

Because of the importance of this problem in gravitation, electrostatics, elasticity, and fluid dynamics, an enormous amount of attention has been given to the development of fast solvers for its solution. "Fast" here means that the CPU time should be proportional or nearly proportional to the number of degrees of freedom used in discretizing the equation. In circular or rectangular domains with regular

grids, methods based on the Fast Fourier transform (FFT) have been shown to be extremely effective. When the domain is more complex or the discretization is non-uniform, however, these methods no longer apply. Thus, there has been a substantial amount of effort aimed at developing methods which can handle highly inhomogeneous source distributions and irregular domains. Direct discretization of the PDE using finite difference or finite element methods has the advantage that it leads to sparse linear systems of equations and these are typically solved iteratively using, say, multigrid or some other preconditioning strategy.

From an analytic perspective, however, it is perhaps more natural to consider integral-equation methods. It is well known, for example, that

$$u_p(\mathbf{x}) = \int_{\mathbb{R}^2} G_L(\mathbf{x}, \mathbf{y}) f(\mathbf{y})\, dy \;, \tag{3}$$

where

$$G_L(\mathbf{x}, \mathbf{y}) = -\frac{1}{2\pi} \log \|\mathbf{x} - \mathbf{y}\| \;, \tag{4}$$

satisfies (1) and that its boundary values are well-defined. Letting $g_p(\mathbf{x})$ be the restriction of u_p to Γ, it is clear that

$$u = u_p + v_p,$$

where $v_p(\mathbf{x})$ satisfies

$$-\Delta v_p(\mathbf{x}) = 0 \quad \text{in } \Omega \tag{5}$$

with Dirichlet boundary conditions

$$v_p(\mathbf{x}) = g(\mathbf{x}) - g_p(\mathbf{x}) \quad \text{on } \Gamma. \tag{6}$$

The determination of v_p can be accomplished using boundary integral-equation methods, which have been shown to be essentially optimal. They require $O(N_b)$ work, where N_b is the number of boundary points and, with suitable quadratures, can achieve very high order accuracy. It is important to note that, using this *potential-theoretic* approach, there are no unknowns in the interior of the domain. Moreover, as we shall see below, error estimation is straightforward, and volume integral operators such as (3) can be applied in linear time, leading to optimal computational complexity using, for example, the fast multipole method (FMM) of [19]. The method of [19], however, was aimed at the solution of the Poisson equation in free space, with a right-hand side $f(\mathbf{x})$ specified as a piecewise polynomial on an adaptive quad-tree discretization of the unit box. In the case where $f(\mathbf{x})$ is known only inside a domain Ω (contained in the interior of the unit box B), the extension of $f(\mathbf{x})$ by zero to $B \setminus \Omega$ yields a discontinuous function and requires excessive adaptive refinement near the boundary Γ to achieve high order accuracy using a piecewise polynomial approximation. One of the contributions of this dissertation is the development of a fast and automatic method for function extension that enforces continuity, dramatically reducing the amount of refinement required (Chapter 2). With this gain in efficiency, the approach presented here is a compelling alternative to the use of body-fitted computational elements, e.g. curved triangles or cut-cells, for which the construction of high order quadratures is difficult.

In many applications, one needs to solve a sequence of Dirichlet boundary value problems in the same domain (with different data $f(\mathbf{x})$ and $g(\mathbf{x})$). In order to permit even faster solution times for such problems, we combine the fast direct solver of [31] for solving (5), (6) with fast volume integral methods. This also

requires the development of a fast algorithm for evaluating layer potentials defined on the boundary Γ at all target points inside the domain Ω (Chapters 1 and 2). For fluid dynamic applications, where the modified Stokes equations play an important role, we also developed a new fast multipole method for the governing Green's function which overcomes the instabilities inherent in existing schemes (Chapter 4). Finally, we have developed a new method for designing quadratures for volume integrals on adaptive quad-tree data structures, which is important when considering the Helmholtz or modified Helmholtz equation (Chapter 3). We illustrate the performance of our fast solvers in Chapter 5 and discuss some open problems in Chapter 6.

Chapter 1

Integral-equation methods

1.1 Mathematical preliminaries

Existence and uniqueness of the solution to an integral equation is often related to the uniqueness of solutions to the corresponding PDE. We collect here some well-known uniqueness results for PDEs which will be needed later. For reference, see, inter alia, [20, 22, 28].

In the following, we consider a bounded domain Ω, possibly multiply-connected, with a smooth boundary Γ. Let the outward normal direction for a point $\mathbf{x}$ on Γ be denoted by $\boldsymbol{\nu}(\mathbf{x})$ and the corresponding positively-oriented unit tangent vector be denoted by $\boldsymbol{\tau}(\mathbf{x})$. We will also consider exterior domains of the form $\Omega_e = \mathbb{R}^2 \setminus \bar{\Omega}$ for sets Ω given as the union of finitely many disjoint, simply-connected domains, where $\bar{\Omega}$ indicates the closure of Ω. The boundary points of Ω_e are the same as those for Ω but the unit normal directions and unit tangent vectors are reversed and we use Γ^*, with $\boldsymbol{\nu}^*(\mathbf{x}) = -\boldsymbol{\nu}(\mathbf{x})$ and $\boldsymbol{\tau}^*(\mathbf{x}) = -\boldsymbol{\tau}(\mathbf{x})$, to make this distinction.

We omit the proofs for the following results concerning the Laplace equation

in two dimensions, as they are standard (relying on maximum principles or energy methods).

Theorem 1.1. *(Uniqueness for the Laplace Dirichlet problem.) If* $u(\mathbf{x})$ *satisfies*

$$\Delta u(\mathbf{x}) = 0 \quad \text{in } \Omega\,, \tag{1.1}$$

$$u(\mathbf{x}) = 0 \quad \text{on } \Gamma\,, \tag{1.2}$$

then $u \equiv 0$ *in* Ω*. Similarly, if* $u(\mathbf{x})$ *satisfies*

$$\Delta u(\mathbf{x}) = 0 \quad \text{in } \Omega_e\,, \tag{1.3}$$

$$u(\mathbf{x}) = 0 \quad \text{on } \Gamma^*\,, \tag{1.4}$$

with $u(\mathbf{x})$ *bounded, then* $u \equiv 0$ *in* Ω_e*.*

In the case of the Neumann problem, uniqueness holds only up to an additive constant, which is clear from the form of the equation.

Theorem 1.2. *(Uniqueness for the Laplace Neumann problem.) If* $u(\mathbf{x})$ *satisfies*

$$\Delta u(\mathbf{x}) = 0 \quad \text{in } \Omega\,, \tag{1.5}$$

$$\partial_\nu u(\mathbf{x}) = 0 \quad \text{on } \Gamma\,, \tag{1.6}$$

then $u \equiv c$ *in* Ω*, for a constant* c*. Similarly, if* $u(\mathbf{x})$ *satisfies*

$$\Delta u(\mathbf{x}) = 0 \quad \text{in } \Omega_e\,, \tag{1.7}$$

$$\partial_{\nu^*} u(\mathbf{x}) = 0 \quad \text{on } \Gamma^*\,, \tag{1.8}$$

with $u(\mathbf{x})$ bounded, then $u \equiv c$ in Ω_e, for a constant c.

It is common in an integral-equation approach to the incompressible Navier-Stokes equations to enforce the boundary conditions by solving the homogeneous modified Stokes equations with appropriate boundary conditions. These equations are given by

$$\begin{aligned} \Delta \mathbf{u} - \alpha^2 \mathbf{u} &= \nabla p \quad \text{in } \Omega \,, & (1.9) \\ \nabla \cdot \mathbf{u} &= 0 \quad \text{in } \Omega \,, & (1.10) \\ \mathbf{u} &= \mathbf{u}_b \quad \text{on } \Gamma \,, & (1.11) \end{aligned}$$

where we have specified velocity boundary conditions. Existence and uniqueness results for these equations are less common in the literature than for the Laplace equation, but they can be found, for instance, in [58].

In proving uniqueness for these equations, it is convenient to introduce some notation. The rate of deformation is denoted by the tensor $\mathbf{e}$ and is defined as

$$e_{ij} = \frac{1}{2} \left(\partial_{x_j} u_i + \partial_{x_i} u_j \right) \,. \tag{1.12}$$

The stress tensor $\boldsymbol{\sigma}$ is then defined by

$$\sigma_{ij} = -p\delta_{ij} + 2e_{ij} \,, \tag{1.13}$$

where δ_{ij} is the standard Kronecker delta. With these definitions, the value

$$\mathbf{f}(\mathbf{x}) = \boldsymbol{\sigma}(\mathbf{x}) \cdot \boldsymbol{\nu}(\mathbf{x}) \,, \tag{1.14}$$

represents the surface traction that the fluid exerts at a point $\mathbf{x}$ on the boundary.

The following lemma forms the basis of an energy method for establishing the uniqueness of solutions to the modified Stokes problem.

Lemma 1.3. *Let* $(\mathbf{u}, p)$ *be a solution of* (1.9), (1.10), (1.11) *and* $\mathbf{f}$ *and* $\mathbf{e}$ *be the tensors defined above. Then*

$$\int_\Gamma u_i f_i \, dS = \int_\Omega \alpha^2 u_i u_i + 2 e_{ij} e_{ij} \, dx \ , \tag{1.15}$$

where we have used the standard Einstein notation for summing over indices of tensors.

It is worth noting that the above lemma makes clear that specifying velocity boundary conditions is an analogue of the Laplace Dirichlet problem and specifying the surface traction $\mathbf{f}$ is an analogue of the Neumann problem.

The following lemmas are standard results and concern harmonic and modified Helmholtz potentials in unbounded domains.

Lemma 1.4. *Let* h *be a bounded harmonic function in the exterior of a disc. Then,* $|\partial_{x_i} h(\mathbf{x})| = \mathcal{O}(1/|\mathbf{x}|^2)$ *and* $|\partial_{x_i}\partial_{x_j} h(\mathbf{x})| = \mathcal{O}(1/|\mathbf{x}|^3)$ *as* $|\mathbf{x}| \to \infty$*, for* $i, j \in \{1, 2\}$*.*

Lemma 1.5. *Let* h *be a function which satisfies*

$$\Delta h - \alpha^2 h = 0 \tag{1.16}$$

and $h(\mathbf{x}) \to 0$ *as* $|\mathbf{x}| \to \infty$ *in the exterior of a disc. If* $h = 0$ *on the boundary of the disc, then* $h \equiv 0$*.*

The following lemma is a consequence of the uniqueness result above, separation of variables, and the properties of modified Bessel functions (section 10.25 of [17]).

Lemma 1.6. *Let h be a function which satisfies*

$$\Delta h - \alpha^2 h = 0 \tag{1.17}$$

and $h(\mathbf{x}) \to 0$ as $|\mathbf{x}| \to \infty$ in the exterior of a disc and let h be a C^1 function on the boundary of the disc. Then, $|h(\mathbf{x})| = \mathcal{O}(e^{-\alpha|\mathbf{x}|})$ as $|\mathbf{x}| \to \infty$.

Theorem 1.7. *Uniqueness for the modified Stokes problem with velocity boundary conditions. If $(\mathbf{u}, p)$ satisfy*

$$\begin{aligned} \Delta\mathbf{u} - \alpha^2\mathbf{u} &= \nabla p \quad \text{in } \Omega\,, & (1.18)\\ \nabla\cdot\mathbf{u} &= 0 \quad \text{in } \Omega\,, & (1.19)\\ \mathbf{u} &= \mathbf{0} \quad \text{on } \Gamma\,, & (1.20) \end{aligned}$$

then $\mathbf{u} \equiv \mathbf{0}$ and $p \equiv c$ in Ω, for some constant c. Similarly, if $(\mathbf{u}, p)$ satisfies

$$\begin{aligned} \Delta\mathbf{u} - \alpha^2\mathbf{u} &= \nabla p \quad \text{in } \Omega_e\,, & (1.21)\\ \nabla\cdot\mathbf{u} &= 0 \quad \text{in } \Omega_e\,, & (1.22)\\ \mathbf{u} &= \mathbf{0} \quad \text{on } \Gamma^*\,, & (1.23) \end{aligned}$$

with $\mathbf{u}(\mathbf{x}) \to \mathbf{0}$ as $|\mathbf{x}| \to \infty$ and p bounded, then $\mathbf{u} \equiv \mathbf{0}$ and $p \equiv c$ in Ω_e, for some constant c.

Proof: For the bounded domain Ω, the proof follows by recognizing that the left hand side of (1.15) is zero and the integrands on the right hand side are positive.

Consider the unbounded domain Ω_e. For sufficiently large R, the set $D = \Omega_e \cap B_R(\mathbf{0})$ contains the boundary Γ^*. In this case, we have

$$\int_D \alpha^2 u_i u_i + 2e_{ij}e_{ij}\,dx = \int_{\partial D} u_i f_i\,dS = \int_{\partial B_R(\mathbf{0})} u_i f_i\,dS\ . \tag{1.24}$$

Let $\omega = \partial_{x_2} u_1 - \partial_{x_1} u_2$ be the vorticity. Then, ω satisfies

$$\Delta\omega - \alpha^2\omega = 0 \quad \text{in } \Omega_e \tag{1.25}$$

and

$$\nabla^\perp \omega = \Delta \mathbf{u}\ , \tag{1.26}$$

where $\nabla^\perp = (\partial_{x_2}, -\partial_{x_1})$. Therefore,

$$\mathbf{u} = \frac{1}{\alpha^2}\left(\nabla^\perp\omega - \nabla p\right)\ . \tag{1.27}$$

Because p is bounded and harmonic, we have $|\nabla p| = \mathcal{O}(1/|\mathbf{x}|^2)$ as $\mathbf{x} \to \infty$. Together with the decay of $\mathbf{u}$, this implies that $\nabla^\perp\omega$ tends to zero at infinity. Further, because ω satisfies (1.25), we have that $\nabla^\perp\omega$ decays exponentially at infinity. Therefore, $|\mathbf{u}| = \mathcal{O}(1/|\mathbf{x}|^2)$ as $\mathbf{x} \to \infty$. Similar reasoning implies that $|\nabla\mathbf{u}| = \mathcal{O}(1/|\mathbf{x}|^3)$ as $|\mathbf{x}| \to \infty$. Finally, this implies that the right-hand-side of (1.24) tends to zero as $R \to \infty$, completing the proof.

□

1.1.1 Free-space Green's functions

For many partial differential equations of physical interest, the solution operator is known for the "free-space" problem. If L is a linear differential operator and f a sufficiently smooth function of compact support, then the free-space problem is to

find u satisfying $Lu = f$ on all of $\mathbb{R}^2$, subject to appropriate conditions at infinity. Typically, the solution operator is given by

$$u(\mathbf{x}) = \int_{\mathbb{R}^2} \Phi(\mathbf{x}, \mathbf{y}) f(\mathbf{y})\, dy \;, \tag{1.28}$$

where Φ is referred to as the free-space Green's function. In the theory of distributions, one writes that $L\Phi(\mathbf{x}, \mathbf{y}) = \delta(\mathbf{x} - \mathbf{y})$.

The Green's functions for the Poisson equation and the modified Helmholtz equation are well-known and presented here without their derivations.

Lemma 1.8. *(Free-space Green's function for the Poisson equation.) Let f be a continuous function of compact support. Then, the function u defined by*

$$u(\mathbf{x}) = \int_{\mathbb{R}^2} G_L(\mathbf{x}, \mathbf{y}) f(\mathbf{y})\, dy \;, \tag{1.29}$$

where

$$G_L(\mathbf{x}, \mathbf{y}) = -\frac{1}{2\pi} \log \|\mathbf{x} - \mathbf{y}\| \;, \tag{1.30}$$

satisfies

$$\begin{aligned} -\Delta u &= f \quad \text{in } \mathbb{R}^2 \;, & (1.31)\\ u(\mathbf{x}) &= -\frac{\log(\mathbf{x})}{2\pi} \int_{\mathbb{R}^2} f(\mathbf{y})\, dy + \mathcal{O}\left(1/\|\mathbf{x}\|\right) \quad \text{as } \|\mathbf{x}\| \to \infty \;. & (1.32) \end{aligned}$$

Lemma 1.9. *(Free-space Green's function for the modified Helmholtz equation.) Let f be a continuous function of compact support. Then, the function u defined by*

$$u(\mathbf{x}) = \int_{\mathbb{R}^2} G_Y(\mathbf{x}, \mathbf{y}) f(\mathbf{y})\, dy \;, \tag{1.33}$$

where

$$G_Y(\mathbf{x},\mathbf{y}) = \frac{1}{2\pi} K_0(\alpha\|\mathbf{x}-\mathbf{y}\|) \;, \tag{1.34}$$

with K_0 the modified Bessel function of the second kind, satisfies

$$-\Delta u + \alpha^2 u = f \quad \text{in } \mathbb{R}^2 \;, \tag{1.35}$$

$$u(\mathbf{x}) \to 0 \quad \text{as } \|\mathbf{x}\| \to \infty \;. \tag{1.36}$$

1.2 Potential theory

In this section we present some facts concerning the functions induced by layer-potentials and the corresponding integral operators. The results can be found in, inter alia, [39]. A treatment which emphasizes the physical interpretation of these objects can be found in [28].

1.2.1 Layer potentials

The free-space Green's functions $G_L(\mathbf{x},\mathbf{y})$ and $G_Y(\mathbf{x},\mathbf{y})$ of the previous section can be thought of as the potential at the point $\mathbf{x}$ due to a unit charge located at $\mathbf{y}$. Accordingly, the potential defined by

$$u(\mathbf{x}) = S\sigma(\mathbf{x}) = \int_\Gamma G_L(\mathbf{x},\mathbf{y})\sigma(\mathbf{y})\, dS(\mathbf{y}) \tag{1.37}$$

represents the potential due to a charge distributed along the curve Γ with density σ. The resulting function is referred to as a single layer potential. When restricted to evaluation points $\mathbf{x}$ on Γ, we use the notation

$$u(\mathbf{x}) = \mathcal{S}\sigma(\mathbf{x}) = \int_\Gamma G_L(\mathbf{x},\mathbf{y})\sigma(\mathbf{y})\, dS(\mathbf{y}) \,, \tag{1.38}$$

where the integral exists as an improper integral.

Theorem 1.10. *The kernel $G_L(\mathbf{x},\mathbf{y})$ is weakly singular on Γ, hence $\mathcal{S}$ is a compact operator on $\mathcal{B} = C(\Gamma)$ and $\mathcal{H} = L^2(\Gamma)$.*

Theorem 1.11. *Let Ω, Γ, Ω_e, and Γ^* be as in the previous section, with Γ of class C^2. Then, the single layer potential is harmonic in Ω and Ω_e and is continuous in $\mathbb{R}^2$. Let $\mathbf{x}_0 \in \Gamma$ and $\boldsymbol{\nu}_0 = \boldsymbol{\nu}(\mathbf{x}_0)$. The limiting values of the normal derivative of the potential satisfy the following jump relations*

$$\lim_{h\to 0^+} \partial_{\nu_0} u(\mathbf{x}_0 \mp h\boldsymbol{\nu}_0) = \pm\frac{1}{2}\sigma(\mathbf{x}_0) + \mathcal{S}'\sigma(\mathbf{x}_0) \tag{1.39}$$

$$= \pm\frac{1}{2}\sigma(\mathbf{x}_0) + \oint_\Gamma \partial_{\nu_0} G_L(\mathbf{x}_0,\mathbf{y})\sigma(\mathbf{y})\, dS(\mathbf{y}) \,, \tag{1.40}$$

where the symbol $\oint$ indicates that the integral is interpreted in the Cauchy principal value sense.

While the kernel of the operator $\mathcal{S}'$ might be expected to have a stronger singularity than the kernel of $\mathcal{S}$, it turns out that for a sufficiently smooth curve this is not the case. We have

Theorem 1.12. *For Γ of class C^2, the kernel $\partial_{\nu_x} G_L(\mathbf{x},\mathbf{y})$ has a removable singularity at $\mathbf{y} = \mathbf{x}$, hence $\mathcal{S}'$ is a compact operator on $\mathcal{B} = C(\gamma)$ and $\mathcal{H} = L^2(\Gamma)$.*

The directional derivative of the free-space Green's function can be thought of as the potential due to a dipole. Accordingly, the potential defined by

$$u(\mathbf{x}) = D\mu(\mathbf{x}) = \int_\Gamma \partial_{\nu_y} G_L(\mathbf{x},\mathbf{y})\mu(\mathbf{y})\, dS(\mathbf{y}) \tag{1.41}$$

represents the potential due to a continuous distribution μ of normally-oriented dipoles along the curve Γ. The resulting function is called a double layer potential. As in the case of $\mathcal{S}'$, the kernel of the double layer potential is not as singular as might be expected when restricted to a sufficiently smooth curve. We have

Theorem 1.13. *For Γ of class C^2, the kernel $\partial_{\nu_y} G_L(\mathbf{x}, \mathbf{y})$ has a removable singularity at $\mathbf{y} = \mathbf{x}$, hence the double layer operator restricted to Γ, $\mathcal{D}$, is a compact operator on $\mathcal{B} = C(\gamma)$ and $\mathcal{H} = L^2(\Gamma)$.*

The jump properties of the double layer potential are summarized in

Theorem 1.14. *Let Ω, Γ, Ω_e, and Γ^* be as in the previous section, with Γ of class C^2. Then, the double layer potential is harmonic in Ω and Ω_e. Let $\mathbf{x}_0 \in \Gamma$ and $\boldsymbol{\nu}_0 = \boldsymbol{\nu}(\mathbf{x}_0)$. The limiting values of the potential satisfy the following jump relations*

$$\lim_{h \to 0^+} u(\mathbf{x}_0 \mp h\boldsymbol{\nu}_0) = \mp\frac{1}{2}\mu(\mathbf{x}_0) + \mathcal{D}\mu(\mathbf{x}_0) \tag{1.42}$$

$$= \mp\frac{1}{2}\mu(\mathbf{x}_0) + \oint\!\!\!\!\!\!\int_\Gamma \partial_{\nu_y} G_L(\mathbf{x}_0, \mathbf{y})\sigma(\mathbf{y})\, dS(\mathbf{y})\,, \tag{1.43}$$

where the integral is again interpreted in the Cauchy principal value sense. Moreover, the limiting values of the normal derivative are continuous across Γ.

Finally, we note that for a general Lipschitz curve Γ, the operators $\mathcal{S}'$ and $\mathcal{D}$ are merely bounded, not necessarily compact, and the integrals in their definitions must be taken in the Cauchy principal-value sense.

1.2.2 Fredholm alternative

The following theorems are adapted from [39]. The second is commonly referred to as the "Fredholm alternative."

Theorem 1.15. *Let $\mathcal{H}$ be a Hilbert space with inner product $\langle \cdot, \cdot \rangle$ and A and B be compact adjoint operators on $\mathcal{H}$. Then the nullspaces of $I - A$ and $I - B$ have the same dimension.*

Theorem 1.16. *(Fredholm alternative.) Let $\mathcal{H}$ be a Hilbert space with inner product $\langle \cdot, \cdot \rangle$ and A and B be compact adjoint operators on $\mathcal{H}$. Then*

$$(I - A)\,\mathcal{H} = N(I - B)^{\perp} \tag{1.44}$$

and

$$(I - B)\,\mathcal{H} = N(I - A)^{\perp}\ , \tag{1.45}$$

where $N(C)$ denotes the nullspace of the operator C and

$$V^{\perp} = \{f \in \mathcal{H} : \langle f, g \rangle = 0 \quad \text{for } g \in V\}\,. \tag{1.46}$$

The Fredholm alternative demonstrates that for a large class of infinite dimensional linear operators the more familiar existence and uniqueness results of linear algebra still hold. A related result is

Theorem 1.17. *Let A be a compact operator on a Hilbert space $\mathcal{H}$. If $(I-A)f = 0$ implies that $f = 0$, then the solution f of $(I - A)f = g$ exists for any g and is unique.*

The preceding theorems also hold in the more general case of a Banach space

$\mathcal{B}$ equipped with a non-degenerate bilinear $(\cdot\,,\cdot)$ or sesquilinear $\langle\cdot\,,\cdot\rangle$ form.

There is a simple extension of the above theorems for certain operators which are not exactly of the form $I - A$ for A compact. Let C be a linear operator. Suppose that there exists a linear operator R_l satisfying $R_l C = I - A_l$, for A_l a compact operator. Such an operator R_l is called a *left regularizer* and, in the case that R_l is injective, R_l is called an *equivalent left regularizer*. It is clear, for R_l an equivalent left regularizer, that $Cx = f$ and $(I - A_l)x = R_l f$ have the same solutions. In particular, Theorem 1.17 still applies for operators C with equivalent left regularizers.

1.2.3 Existence-uniqueness example

In this section, we present an existence-uniqueness proof for an integral representation of the solution to the interior Neumann problem of the Laplace equation. This specific example is included because it demonstrates the use of Theorem 1.17 in a simple setting and it is somewhat non-standard.

Let Ω and Γ be as above, with Γ of class C^2. We aim to solve the interior Neumann problem

$$\Delta u = 0 \quad \text{in } \Omega\,, \tag{1.47}$$

$$\partial_\nu u = g \quad \text{on } \Gamma\,, \tag{1.48}$$

for continuous data g. An application of the divergence theorem shows that the data g must satisfy the compatibility condition

$$\int_\Gamma g(\mathbf{y})\, dS(\mathbf{y}) = 0\ , \tag{1.49}$$

for a solution u to exist. Further, we have that solutions u are unique by Theorem 1.2.

To find u, we represent the solution as a single layer potential $u = S\sigma$. Using the jump relations of Theorem 1.11, we find that the boundary conditions imply

$$\frac{1}{2}\sigma(\mathbf{x}) + \mathcal{S}'\sigma(\mathbf{x}) = g(\mathbf{x}) \tag{1.50}$$

for $\mathbf{x}$ on Γ.

We will make use of the following well-known results. A proof of the first can be found in [28] and the second follows from standard multipole estimates.

Theorem 1.18. *(Gauss' theorem). For Γ of class C^2,*

$$\int_\Gamma \partial_{\nu_y} G_L(\mathbf{x},\mathbf{y})\, dS(\mathbf{y}) = \begin{cases} -1, & \mathbf{x} \in \Omega \\ -\dfrac{1}{2}, & \mathbf{x} \in \Gamma \\ 0, & \mathbf{x} \in \Omega_e \end{cases} . \tag{1.51}$$

Lemma 1.19. *If $\int_\Gamma \sigma(\mathbf{y})\, dS(\mathbf{y}) = 0$, then $S\sigma(\mathbf{x}) \to 0$ as $\|\mathbf{x}\| \to \infty$.*

Instead of (1.50), we consider the following integral equation for σ. Let

$$\frac{1}{2}\sigma(\mathbf{x}) + \mathcal{S}'\sigma(\mathbf{x}) + \mathcal{W}\sigma(\mathbf{x}) = g(\mathbf{x})\ , \tag{1.52}$$

where

$$\mathcal{W}\sigma(\mathbf{x}) = \int_\Gamma \sigma(\mathbf{y})\, dS(\mathbf{y})\ . \tag{1.53}$$

In the case that g satisfies the compatibility condition, the above results imply that solutions of (1.52) satisfy $\int_\Gamma \sigma(\mathbf{y})\, dS(\mathbf{y}) = 0$ and are therefore also solutions to (1.50). Because $\mathcal{W}$ and $\mathcal{S}'$ are compact on $C(\Gamma)$, Theorem 1.17 applies.

Let σ_v satisfy

$$\frac{1}{2}\sigma_v(\mathbf{x}) + \mathcal{S}'\sigma_v(\mathbf{x}) + \mathcal{W}\sigma_v(\mathbf{x}) = 0\ . \tag{1.54}$$

As noted above, this implies that $\int_\Gamma \sigma_v(\mathbf{y})\, dS(\mathbf{y}) = 0$ and

$$\frac{1}{2}\sigma_v(\mathbf{x}) + \mathcal{S}'\sigma_v(\mathbf{x}) = 0\ . \tag{1.55}$$

If $v = S\sigma_v$, then v satisfies the interior Neumann problem with zero boundary data. Therefore, $v \equiv c$ in Ω. Because $S\sigma_v$ is continuous in $\mathbb{R}^2$, the potential v satisfies the exterior Dirichlet problem with $v \equiv c$ on Γ and v is bounded in Ω_e. Therefore, $v \equiv c$ in Ω_e. This implies that the jump in the normal derivative of v is zero across the boundary Γ and by the jump conditions for the single layer potential we have $\sigma_v \equiv 0$ on Γ.

By Theorem 1.17, we have that solutions of (1.52) exist and are unique.

1.2.4 Spectral properties

The following theorem is adapted from [39] and characterizes the spectrum of a compact operator.

Theorem 1.20. *Let A be a compact operator on an infinite dimensional Hilbert space $\mathcal{H}$. Then $\lambda = 0$ belongs to the spectrum $\sigma(A)$ and the set $\sigma(A) \setminus \{0\}$ is countable with $\lambda = 0$ as the only possible accumulation point.*

A direct consequence of the above theorem is that the spectrum of $\beta - A$ clusters around β. Further, if $\beta - A$ is invertible, the continuous operator has a finite condition number. For a well-chosen discretization, the condition number of the resulting linear system is bounded, independent of the mesh spacing and the solutions of the integral equation are stable under perturbations.

1.3 Solving the homogeneous problem

In the previous sections, we have seen how to recast a homogeneous partial differential equation as an integral equation through the use of layer potentials. While the properties of the associated operators are indeed favorable to discretization, the numerical solution of these equations requires some care. In particular, the integral equations often include singular kernels which need non-standard quadrature rules. We discuss some of the literature in this area in Section 1.3.1. Once discretized, the result is a dense linear system. A naïve approach would require $\mathcal{O}(N^3)$ work for a system with N unknowns, which is undesirable for large-scale problems. We discuss fast solution methods available for these systems in Section 1.3.2. Finally, once the solution of the integral equation is found, the layer potential must be evaluated inside the domain. This step can be difficult for evaluation points near the boundary of the domain, as the integral kernel is near-singular. We discuss methods for near boundary evaluation points in Section 1.3.3.

1.3.1 Discretization of integral equations

To discretize an integral equation for numerical solution, we use a Nyström approach. In particular, we represent the data and the solution by their values at

points on the curve Γ which are used for an integration rule [5, 39]. The Galerkin method, by contrast, represents the data and the solution by their orthogonal projections onto finite-dimensional subspaces (here, the underlying function space is typically taken to be a Hilbert space). For more on the Galerkin method, see [29, 39].

The basis of a Nyström method is a numerical quadrature of the integral operator on the curve Γ. Typically, different integration rules are required for smooth, weakly singular, and singular integral kernels.

One popular scheme is to define points on the curve which are either equispaced in arc length or equispaced in terms of an underlying parameterization. For smooth integral kernels, the trapezoidal rule can be applied with spectral accuracy. The locally compensated rules of [1] and [35] are available for weakly singular kernels, with high order accuracy (e.g. 16th order). For certain singular integrals, the alternating-point trapezoidal rule of [65] provides a spectrally accurate quadrature.

To facilitate adaptivity, we use quadrature rules based on dividing the curve Γ into panels, with scaled Legendre nodes on each panel as collocation points. For smooth integral kernels, the standard Gaussian quadrature rule is high order accurate. For singular kernels, so-called generalized Gaussian quadrature rules can be computed [11, 38, 44], which use optimization methods to design high order rules that take the singularity into account.

For integral equations of the second kind, there are surprisingly strong statements available concerning the condition numbers of the linear system resulting from Nyström discretization. Adapted from [39] (see also, [3]), we have

Theorem 1.21. *For the Nyström method applied to a second kind integral equation, the condition numbers for the linear system are uniformly bounded.*

This theorem hints that the linear systems arising from the Nyström method are essentially as well-conditioned as the continuous integral operator they approximate. Another consequence of this theorem is that there is no cost in terms of stability in using more discretization points than necessary to resolve the problem.

1.3.2 Fast solution methods for boundary integral equations

Many integral equations, and their corresponding Nyström approximations, have favorable spectral properties for solution with iterative solvers, e.g. the generalized minimum residual (GMRES) method of [64]. Such methods can be combined with a fast matrix-vector multiplication routine to compute a solution of the linear system, often with optimal computational complexity. The fast multipole method [27] supplies a fast matrix vector multiplication routine, and with GMRES, results in a $\mathcal{O}(N)$ solution method, since the number of iterations required is independent of N (a version of the FMM is described in Section 1.4).

For geometrically complex boundaries, however, the iterative solution methods can behave poorly even if the number of iterations is formally independent of N. In some settings, this problem can be circumvented with a sufficiently good preconditioner. (See, for instance, the impressive Laplace solver of [50], which can handle nearly arbitrary planar domains.) Another option for geometrically complex problems is to avoid the problem of unpredictable iteration counts altogether and make use of "fast direct solvers".

A fast direct solver is characterized by a precomputation step which creates a hierarchical data structure that permits the inverse of the given matrix to be applied rapidly. For the solver to be considered fast, both the precomputation and

the application of the inverse should have a computational complexity of $\mathcal{O}(N^\alpha)$ or $\mathcal{O}(N \log N)$ for N discretization points, with $1 \leq \alpha < 2$.

We will not review the fast direct solver literature here, but we will note that the solvers for non-oscillatory problems can be divided into two broad categories. Both categories make use of the fact that the off-diagonal blocks of system matrices corresponding to integral equations are well-approximated using low rank decompositions. This property is commonly referred to as the "data-sparsity" of such systems. The first category uses the data-sparsity of the system and auxiliary variables to approximate the original system by a larger sparse system, which can be solved rapidly using black-box routines. An example of such a solver is the recursive-skeletonization scheme of [31], which uses the sparse LU package `UMFPACK` [15, 16]. The second category of fast direct solvers do not leverage black-box routines for sparse systems. Instead, the solvers are tailored to the low rank structure of the original linear system. An example of the second category is the method of [2], which factorizes the system into a product of matrices, each of which can be rapidly inverted using the Sherman-Woodbury-Morrison formula. Finally, we note that the application of the inverse is typically much faster than the precomputation, so that fast direct solvers are particularly appealing in settings where the solution is desired for many different right-hand-sides.

1.3.3 Evaluating layer potentials

Once the solution of an integral equation is computed, it remains to evaluate the corresponding layer potential at the desired points in the domain. This step can be complicated by the fact that the integral kernel is near singular for evaluation points near the boundary of the domain. There have been recent developments

in this area and we present some details of the quadrature-by-expansion (QBX) method of [37] here. We mention also the approach developed in [6, 30, 51], which can be more efficient than QBX, but is currently limited to two dimensions.

For concreteness, we consider the use of QBX to evaluate the single layer potential for the Laplace equation, $u = S\sigma$, where S is as defined in (1.37) and σ is taken to be real valued. Let Γ be discretized into panels of Legendre nodes, as in the case of a Nyström discretization of the integral equation for σ. Let $B_r(\mathbf{c})$ (the disc of radius $r > 0$ about a point $\mathbf{c}$) be contained in the domain and let the potential u be given as the real part of a complex power series there about the point $\mathbf{c}$, i.e. let

$$u(\mathbf{x}) = \mathrm{Re}\left(\sum_{l=0}^{\infty} \alpha_l (z-\xi)^l\right) , \tag{1.56}$$

where $\mathbf{x}$ is in $B_r(\mathbf{c})$, $z = x_1 + ix_2$, and $\xi = c_1 + ic_2$. Using standard multipole results, we have that

$$\alpha_0 = -\frac{1}{2\pi}\int_\Gamma \log\|\mathbf{c}-\mathbf{y}\|\sigma(\mathbf{y})\, dS(\mathbf{y}) , \tag{1.57}$$

$$\alpha_l = \frac{1}{2\pi l}\int_\Gamma \frac{\sigma(\mathbf{y})}{(y_1 + iy_2 - \xi)^l}\, dS(\mathbf{y}) \quad \text{for } l \geq 1 . \tag{1.58}$$

From here, the QBX method for evaluating $S\sigma$ is based on two observations. The first is that for a center $\mathbf{c}$ sufficiently far from the boundary, the integrals for the α_l can be computed to high accuracy using the standard Gaussian weights on Γ. The second is that if the sum in (1.56) is truncated after p terms, the error for the exact coefficients α_l is bounded by a constant times r^{p+1}. This error is of course small for small values of r. When using the truncated sum and approximate

coefficients to evaluate at a point near the boundary, we see that these two sources of error are in conflict, i.e. that if we move the center further from the boundary to improve the computed α_l, then the error due to r^{p+1} will increase.

The theoretical foundation for QBX is based on the following theorem (Section 4 of [18] and Theorem 1 in [37]).

Theorem 1.22. *Let Γ be a smooth, bounded curve in the plane. Suppose that $B_r(\mathbf{c})$ is a disc of radius r about $\mathbf{c}$ and that $\overline{B_r(\mathbf{c})} \cap \Gamma = \mathbf{x}$. Assume Γ is divided into panels of length h with $q \geq 1$ scaled Legendre nodes and let $\hat{\alpha}_l$ be the approximations of the coefficients α_l as defined in (1.57), (1.58) using the Gaussian quadrature rule scaled to these panels. For $0 < \beta < 1$, there are constants $C_{p,\beta}$ and $\overline{C}_{p,q,\beta}$ such that if σ is in the Hölder space $C^{p,\beta}(\Gamma) \cap C^{2q,\beta}(\Gamma)$, then*

$$\left| S\sigma(\mathbf{x}) - \sum_{l=0}^{p} \hat{\alpha}_l (z-\xi)^l \right| \leq C_{p,\beta} r^{p+1} \|\sigma\|_{C^{p,\beta}(\Gamma)} + \overline{C}_{p,q,\beta} \left(\frac{h}{4r}\right)^{2q} \|\sigma\|_{C^{2q,\beta}(\Gamma)} , \quad (1.59)$$

where $z = x_1 + ix_2$ and $\xi = c_1 + ic_2$.

The theorem above makes the interplay of the two sources of error, the truncation error and the quadrature error, explicit. In particular, if $r = h$ we have an error term of the form

$$C_{p,\beta} h^{p+1} \|\sigma\|_{C^{p,\beta}(\Gamma)} + \overline{C}_{p,q,\beta} \left(\frac{1}{4}\right)^{2q} \|\sigma\|_{C^{2q,\beta}(\Gamma)} , \quad (1.60)$$

so that the error is of order $p+1$ up to the tolerance $(1/4)^{2q}$. This bound does not give a method which is convergent in the traditional sense, i.e. the error does not tend to zero as h tends to zero, but rather the bound is proportional to the absolute accuracy of the calculation (given by the second term) for small h. In

many implementations of QBX, the density is oversampled on the panels in order to make the second term more manageable. If a traditionally convergent method is desired, one can take $r = \sqrt{h}$, for example.

The QBX method can be accelerated using the fast multipole method, as shown in [62], and can be used for a variety of kernels.

1.4 Outline of a fast multipole method

In this section, we present an outline of the fast multipole method (FMM) on a level-restricted tree. The discussion in this section follows the presentation of [19] and is included here largely for subsequent reference. In particular, the new FMMs discussed in this thesis are essentially the same in structure, so that those algorithms are easily explained by highlighting their differences.

In [19], the FMM is used to compute the volume integral

$$u(\mathbf{x}) = -\frac{1}{2\pi} \int_{\Omega} \log(\|\mathbf{x} - \mathbf{y}\|) f(\mathbf{y})\, dy \,, \tag{1.61}$$

where Ω is the unit box $[-1/2, 1/2] \times [-1/2, 1/2]$, for a continuous source distribution f. For reasons explained below, the FMM is particularly efficient in terms of work per grid point in this context and we will refer to such volume integral codes as "box codes". We will note places where this algorithm can be modified to handle point sources, with some cost in efficiency.

As the components of the algorithm are described, we include relevant snippets of pseudocode. These snippets are given in order and together form a pseudocode for the FMM algorithm as a whole.

1.4.1 Quad-tree and interaction lists

We assume that the domain Ω is to be divided into boxes and on each box the density f will be represented by its values on a box-centered 4×4 grid of equispaced collocation points (this can be generalized to higher order grids rather simply, see [19] for details). In addition, the target points $\mathbf{x}$ in (1.61) are taken to be these same collocation points. For the FMM, these boxes must be arranged in a hierarchical division of space, in particular they are taken to be the leaf boxes of a quad-tree. Let the computational domain Ω be the root box of the tree at level 0. A *quad-tree* is defined recursively, with new boxes at level $l+1$ obtained by subdividing a box at level l into four equal parts. New boxes created in this way are called the children of the box from which they are subdivided (in turn, that box is called their parent).

We allow boxes to be subdivided in an adaptive manner, normally determined by how well the local tensor grid resolves the density f, i.e. if f is not resolved on a given box, then subdivide. (For point sources, a common subdivision criterion is to divide a box if it contains more than a certain maximum number of sources. In this way, different regions of Ω are allowed to have different levels of refinement.) In order to reduce the number of possible neighbor interactions, we impose the restriction that no two leaf boxes which share a boundary point be more than one refinement level apart. Such an adaptive tree is called *level-restricted*.

Following [19], we define several types of boxes relevant to a given box B in the quad-tree.

Definition 1.1.

- A *colleague* is a box at the same level as B which shares a boundary point with B. A box is considered a colleague of itself.

- For B a leaf box, a *coarse neighbor* is a leaf box at a refinement level coarser than B's which shares a boundary point with B.
- For B a leaf box, a *fine neighbor* is a leaf box at a refinement level finer than B's which shares a boundary point with B.
- The *neighbors* of B are given as the union over the colleagues which are leaf boxes, coarse neighbors, and fine neighbors.
- For B a leaf box, the *fine interaction list* of B consists of any children of a colleague of B which are not fine neighbors of B.
- The *interaction region* is the area covered by the neighbors of B's parent excluding the area covered by B's neighbors.
- The *interaction list* consist of the boxes in the interaction region of B which are at the same level as B or are leaf boxes at a coarser level than B.
- The *coarse interaction list* consists of those leaf boxes in the interaction list which are at a coarser level than B.

See Figure 1.4.1 for an illustration. We also introduce the definition of a well-separated box.

Definition 1.2. A box B' is said to be *well-separated* from a given box B if its interior does not intersect the interior of any of the colleagues or neighbors of B.

Any box in the interaction region of B is well-separated from B. The box B is well-separated from boxes in the interaction list at the same level as B but B is not well-separated from boxes in the coarse interaction list. The box B is

well-separated from the boxes in its fine interaction list, but the boxes in the fine interaction list are not well-separated from B.

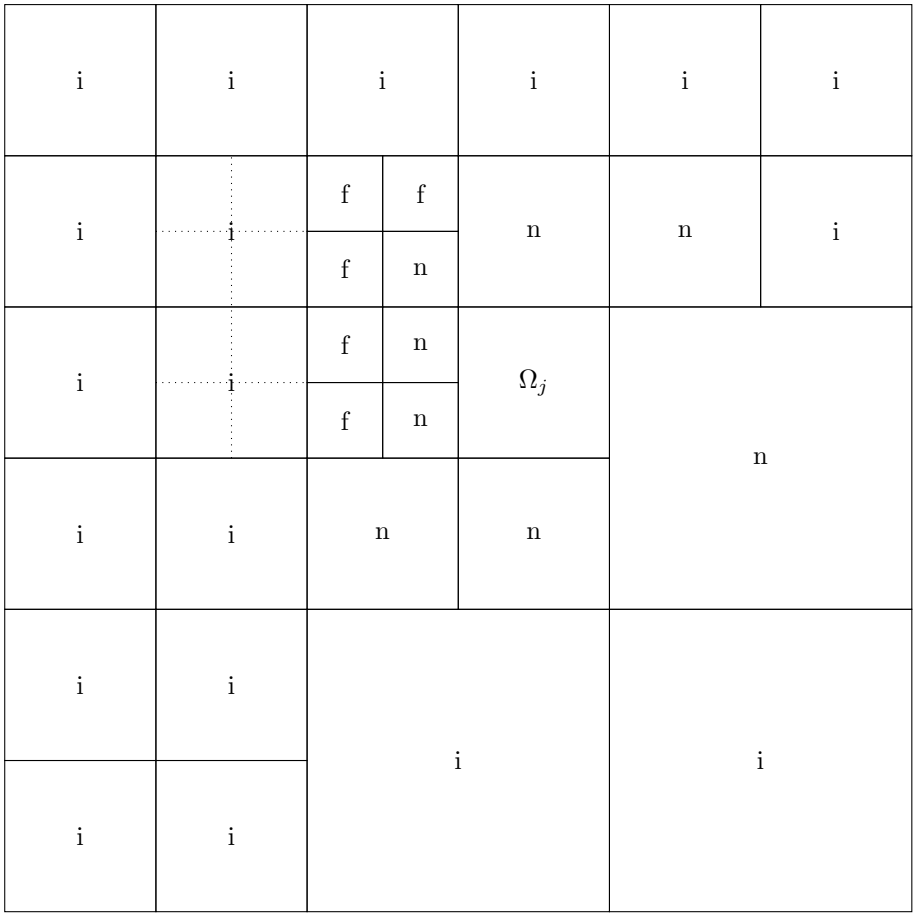

Figure 1.1: Adapted from [19]: an example of the possible local arrangement of boxes for a leaf box Ω_j. Per Definition 1.1, neighbor boxes are labeled with "n", boxes in the interaction list are labeled with "i", and boxes in the fine interaction list are labeled with "f". The dotted lines indicate that some boxes outside the neighbors may have children.

Denote the leaf nodes of the quad-tree by Ω_i for $i = 1, \ldots, M$ (this gives $N = 16M$ collocation points). Then, $\Omega = \cup_{i=1}^{M} \Omega_i$ and

$$u(\mathbf{x}) = \sum_{i=1}^{M} -\frac{1}{2\pi} \int_{\Omega_i} \log(\|\mathbf{x} - \mathbf{y}\|) f(\mathbf{y})\, dy \,. \tag{1.62}$$

Let $\mathbf{x} \in \Omega_j$ for some j. The box code computes (1.62) by adding the contributions from neighbors of Ω_j directly and using the FMM for the remaining summands.

Now that the data structure has been described, we fix the notation for the pseudocode. Assume that we are given an adaptive hierarchical quad-tree structure with L levels for which Ω is the root box $B_{0,0}$. Let the jth box at level l be designated by $B_{l,j}$. Let $a_i^{(l,j)}$ store the multipole coefficients for the density restricted to $B_{l,j}$ and $b_i^{(l,j)}$ store the local expansion coefficients due to well-separated interactions. Let $c_k^{(l,j)}$ store the polynomial coefficients of the local approximation to the density f if $B_{l,j}$ is a leaf box.

1.4.2 Quadrature tables

The processing of local interactions is particularly fast for a box code in comparison with a standard FMM. This is because, up to scale, there are a limited number of possible interactions, and these can be precomputed and stored. This section describes how these interactions are handled.

For a leaf box B with center (ξ, η), let $\mathbf{f}$ denote the values of the density f on the 4×4 grid of collocation points on B. Given the values $\mathbf{f}$, it is simple to compute a fourth order accurate approximation to f on B by performing a least squares fit with functions of the form $\sum_k c_k p_k(y_1 - \xi, y_2 - \eta)$, where the basis functions p_k are taken from the set $\{y_1^m y_2^n : m, n \geq 0, m + n \leq 3\}$ in the standard order (there are 10 such functions). The map from values $\mathbf{f}$ to coefficients $\mathbf{c}$ is the same for each box (up to scale) and can be precomputed and stored.

Let B' be a neighbor box of B and $\mathbf{x}_q$ be a collocation point on B'. If ϕ_B is the potential induced by the density f restricted to B, then we have, to fourth order,

Algorithm 1 FMM on a level-restricted tree (initialization)

for all boxes $B_{l,j}$ **do**
  $\mathbf{a}^{(l,j)} \leftarrow \mathbf{0}$
  $\mathbf{b}^{(l,j)} \leftarrow \mathbf{0}$
  if $B_{l,j}$ is childless **then**
    compute coefficients $\mathbf{c}^{(l,j)}$
    $\hat{u}(\mathbf{x}_q) \leftarrow 0$ for each grid point $\mathbf{x}_q$
  end if
end for

$$\begin{aligned}
\phi_B(\mathbf{x}_q) &= -\frac{1}{2\pi}\int_B \log(\|\mathbf{x}_q - \mathbf{y}\|) f(\mathbf{y})\, dy && (1.63)\\
&\approx \sum_{k=1}^{10} c_k \left(-\frac{1}{2\pi}\int_B \log(\|\mathbf{x}_q - \mathbf{y}\|) p_k(y_1 - \xi, y_2 - \eta)\, dy \right) && (1.64)\\
&= \sum_{k=1}^{10} c_k G_k^B(\mathbf{x}_q)\ . && (1.65)
\end{aligned}$$

Because the logarithm satisfies

$$\log(a\|\mathbf{x} - \mathbf{y}\|) = \log(a) + \log(\|\mathbf{x} - \mathbf{y}\|), \tag{1.66}$$

the local interactions for any size box may be obtained from the local interactions on a reference box by simple rescaling. Further, the 10 functions G_k^B are only ever evaluated at the 16 collocation points of each neighbor box. In all, there are only 16×10 possible values for the G_k^B functions on each of the 9 possible colleague interactions, 12 possible fine neighbor interactions, and 12 possible coarse neighbor interactions. The values of the G_k^B can therefore be precomputed for a reference box with a high precision scheme and stored.

With these precomputations, the values of ϕ_B at the collocation points of B's

neighbors are obtained at the cost of a small matrix-vector multiply. This is in contrast with schemes for computing (1.61) based, for example on unstructured triangulations. In that setting, the local interactions may have to be computed by an expensive adaptive integration technique. We also note that in the case of an FMM with arbitrary point sources and targets this kind of precomputation is unavailable and the direct computation of these interactions involves more expensive kernel evaluations on the fly.

1.4.3 Multipole and local expansions

For efficiently computing interactions between boxes which are not neighbors, the FMM makes use of multipole and local expansions. In this section, we omit proofs and present only the relevant results. For a thorough treatment, see [24, 27]. For such expansions, we will often associate a point in the real plane $\mathbf{x} = (x_1, x_2)$ with the corresponding point $x_1 + ix_2$ in the complex plane.

Let B be a leaf box with center (ξ, η) and let c_k be the coefficients of f restricted to B, as in the last section. The potential ϕ_B induced by f restricted to B, has a multipole expansion defined by

$$\phi_B(\mathbf{x}) = a_0 \log|z - w| + \mathrm{Re}\left(\sum_{l=1}^{\infty} \frac{a_l}{(z-w)^l}\right) , \tag{1.67}$$

where $z = x_1 + ix_2$ and $w = \xi + i\eta$ and the coefficients a_l are given by

$$\begin{aligned} a_0 &= -\frac{1}{2\pi} \int_B f(\mathbf{y})\, dy & (1.68)\\ &\approx -\frac{1}{2\pi} \sum_{k=1}^{10} c_k \int_B p_k(\mathbf{y})\, dy\ , & (1.69) \end{aligned}$$

$$a_l = -\frac{1}{2\pi l}\int_B (y_1 + iy_2 - w)^l f(\mathbf{y})\,dy \tag{1.70}$$

$$\approx -\frac{1}{2\pi l}\sum_{k=1}^{10} c_k \int_B (y_1 + iy_2 - w)^l p_k(\mathbf{y})\,dy\ . \tag{1.71}$$

Within the box code, the approximations noted above are used for the coefficients. For $\mathbf{x}$ in a well-separated box, the error due to truncating the expansion (1.67) after p terms and using the approximate a_k is bounded by

$$\left(\frac{1}{2}\right)^p \frac{1}{2\pi}\int_B |f(\mathbf{y})|\,dy + \frac{1}{2\pi}\int_B \log|\mathbf{x}-\mathbf{y}|\left|f(\mathbf{y}) - \sum_{k=1}^{10} c_k p_k(y_1-\xi, y_2-\eta)\right| dy\ . \tag{1.72}$$

As in the case of the local interactions, many of the values needed to form the multipole coefficients can be precomputed. Indeed, the values

$$\int_B (y_1 + iy_2 - w)^l p_k(\mathbf{y})\,dy \tag{1.73}$$

are the same for each box (up to scale) and can therefore be stored for some reference box. This reduces the cost of forming the multipole coefficients to a small $(p+1)\times 10$ matrix-vector multiply.

For domains with irregular elements, these integrals would again have to be handled on a case-by-case basis, though the integrand is no longer singular. In the case of point sources, the contribution from each source would have to be computed separately.

The potential induced by a charge density which is contained only in boxes well-separated from a given box B can be represented by a local expansion Ψ_B on

B. These expansions take the form of a power series

$$\Psi_B = \mathrm{Re}\left(\sum_{k=0}^{\infty} b_k (z-w)^k\right) . \tag{1.74}$$

In the FMM, the coefficients b_k are obtained via translations of local expansion coefficients at higher levels and applying multipole-to-local translation operators to the multipole expansions of well-separated boxes in the interaction list.

1.4.4 Far field interactions and translation operators

The FMM relies on results from potential theory to translate both multipole and local expansions and to convert multipole expansions into local expansions. Together with the adaptive quad-tree structure, these results are what allow the FMM to be an $\mathcal{O}(N)$ algorithm. Again, we omit the proofs and present some of the relevant results for later reference. These results are drawn directly from [27].

For a box with children, the multipole coefficients due to the charge density restricted to that box can be obtained from the multipole coefficients of its children. The procedure for merging the coefficients of the children into coefficients for the parent is based on the following formula for shifting the center of a multipole expansion.

Lemma 1.23. *(Adapted from Lemma 2.3 of [27].) Suppose that*

$$\phi(z) = a_0 \log(z - z_0) + \sum_{l=1}^{\infty} \frac{a_l}{(z-z_0)^l} \tag{1.75}$$

is a multipole expansion of the potential due to a charge density which is contained inside the disc of radius R about z_0. Then, for z outside the disc of radius $R + |z_0|$ about the origin

$$\phi(z) = b_0 \log(z) + \sum_{l=1}^{\infty} \frac{b_l}{z^l} \,, \tag{1.76}$$

where $b_0 = a_0$ *and*

$$b_l = \left(\sum_{m=1}^{l} a_m z_0^{l-m} \binom{l-1}{m-1} \right) - \frac{a_0 z_0^l}{l} \,, \tag{1.77}$$

using the standard notation for binomial coefficients. We also have the following bound for the truncation error. With $p \geq 1$*,*

$$\left| \phi(z) - b_0 log(z) - \sum_{l=1}^{p} \frac{b_l}{z^l} \right| \leq \frac{F/2\pi}{1 - (|z_0| + R)/|z|} \left(\frac{|z_0| + R}{|z|} \right)^{p+1} \,, \tag{1.78}$$

where F *is the* L_1 *norm of the density.*

It is now possible to compute a multipole expansion for each box in the tree hierarchy which represents the potential due to the charge density restricted to that box. Starting from the lowest level and working up the tree, the expansion can be formed by (a) calling the multipole formation procedure of the previous section for a childless box or (b) merging the multipole expansions already computed for the children of the given box.

Once all of the multipole expansions have been formed, we move on to forming local expansions in each box. In the FMM, this accomplished using the following formula for converting a multipole expansion into a local expansion.

Lemma 1.24. *(Adapted from Lemma 2.4 of [27].) Suppose that a charge density is contained inside the disc of radius* R *about* z_0 *with* $|z_0| > (1+c)R$ *for some* $c > 1$*. Let the multipole expansion due to this density be given as in Lemma 1.23. Then,*

Algorithm 2 FMM on a level-restricted tree (upward sweep)

```
for l = L, ..., 0 do
    for all boxes j on level l do
        if box B_{l,j} is childless then
            compute the multipole coefficients a^{(l,j)} via (1.69) and (1.71)
        else
            merge multipole coefficients from children via Lemma 1.23
        end if
    end for
end for
```

this multipole expansion converges inside the disc of radius R about the origin and can be represented by a power series there:

$$\phi(z) = \sum_{l=1}^{\infty} b_l z^l \tag{1.79}$$

where,

$$b_0 = \sum_{m=1}^{\infty} \frac{a_m}{z_0^m} (-1)^m + a_0 \log(-z0) \ , \tag{1.80}$$

and

$$b_l = \frac{1}{z_0^l} \left(\sum_{m=1}^{\infty} \frac{a_m}{z_0^m} \binom{l+m-1}{m-1} (-1)^m \right) - \frac{a_0}{z_0^l \ l} \ , \tag{1.81}$$

for $l \geq 1$. There is a similar error bound for this lemma, see [27] for details. Suppose that the charge density is supported in a box and the evaluation points z are taken in another. In the case that these two boxes are well separated from each other, we have

$$\left| \phi(z) - \sum_{l=0}^{p} b_l z^l \right| \leq CF \left(\frac{1}{2} \right)^p \ , \tag{1.82}$$

where F is as in Lemma 1.23 and C is a constant.

Let B be a box in the tree hierarchy. For now, we assume that the part of the local expansion in B due to boxes outside of the interaction region can be obtained in a later step. Consider boxes in the interaction list which are at the same level as B. The contribution to the local expansion for each box B' in this set can be computed by applying the multipole-to-local operation to the multipole coefficients for B'.

Note that boxes in the coarse interaction list of B are necessarily leaf boxes and not well-separated. The contribution due to a box B' in the coarse interaction list can be computed by observing that children of B' *would be* well-separated from B. It is therefore possible to compute multipole expansions for the "ghost" children of B' and convert those into local expansions on B.

Algorithm 3 FMM on a level-restricted tree (process interaction list)

```
for all boxes B_{l,j} do
    for all boxes B' in the interaction list of B_{l,j} do
        if B' is on the same level as B_{l,j} then
            b^{(l,j)} ← b^{(l,j)} + contribution from B' via Lemma 1.24
        else
            b^{(l,j)} ← b^{(l,j)} + contribution from B' using "ghost" children
        end if
    end for
end for
```

Generally, the process of converting multipole expansions to local expansions is one of the more expensive steps in the FMM. This is because (a) there can be many (up to 27) such operations per box and (b) the translation operator is dense, taking $\mathcal{O}(p^2)$ work to map between expansions of length p. The implementation of [19] makes use of plane-wave expansions which can be translated using $\mathcal{O}(p)$ operations. The details are somewhat technical and we refer the interested reader

to [19, 33].

Finally, we present the formula for translating local expansions.

Lemma 1.25. *(Adapted from Lemma 2.5 in [27]) Let z_0, z, and a_l for $l = 0, 1, \ldots, p$ be complex. Then*

$$\sum_{l=0}^{p} a_l (z - z_0)^l = \sum_{m=0}^{p} \left(\sum_{l=m}^{p} a_l \binom{l}{m} (-z_0)^{l-m} \right) z^m \,. \tag{1.83}$$

This formula is exact.

Suppose that for each box B in the hierarchy, the contribution of each box B' in B's interaction list to the local expansion for B has already been computed. For boxes at level 2 and above, there are not any boxes outside the interaction list. Therefore, the local expansion for boxes at these levels already includes the contribution of all well-separated boxes. For a box B at level l, assume that the local expansion of its parent includes the contribution from all well-separated boxes. Then, by shifting the local expansion of the parent and adding it to the local expansion at B due to boxes in B's interaction list results in an expansion at B due to all well-separated boxes. By passing down the levels of the tree, all of the local expansions can be updated in this way.

Algorithm 4 FMM on a level-restricted tree (downward sweep)

```
for all boxes B_{l,j} do
    for all boxes B' in the interaction list of B_{l,j} do
        if B' is on the same level as B_{l,j} then
            b^{(l,j)} ← b^{(l,j)} + contribution from B' via Lemma 1.24
        else
            b^{(l,j)} ← b^{(l,j)} + contribution from B' using "ghost" children
        end if
    end for
end for
```

We note that the procedures and formulas from this section are unaffected by whether the FMM is used for charge densities or point sources.

1.4.5 Computing the potential

For a box B, let ϕ_B be the multipole expansion due to the charge density restricted to B and let Ψ_B be the local expansion due to all well-separated boxes. For a leaf box Ω_i, we denote the set of neighbors by

$$\mathcal{N}(i) = \{j : \Omega_j \text{ is a neighbor of } \Omega_i\} \tag{1.84}$$

and the fine interaction list by

$$\mathcal{F}(i) = \{j : \Omega_j \text{ is in the fine interaction list of } \Omega_i\} \ . \tag{1.85}$$

Let $\mathbf{x}_q$ be a collocation point in Ω_i. Then the value of $u(\mathbf{x}_q)$ in (1.61) can be approximated by the computed value $\hat{u}(\mathbf{x}_q)$ which results from the sum

$$\hat{u}(\mathbf{x}_q) \quad = \quad \sum_{j \in \mathcal{N}(i)} \sum_{k=1}^{10} c_k^{(j)} G_k^{(j)}(\mathbf{x}_q) + \sum_{j \in \mathcal{F}(i)} \phi_{\Omega_j}(\mathbf{x}_q) + \Psi_{\Omega_i}(\mathbf{x}_q) \ . \tag{1.86}$$

1.4.6 Error analysis

Let the function $\tilde{f}$ be defined by the piecewise polynomial approximation to f on each leaf box, i.e., for $\mathbf{x} = (x_1, x_2)$ in Ω_j with center (ξ_j, η_j),

$$\tilde{f}(\mathbf{x}) = \sum_{k=1}^{10} c_k^{(j)} p_k(x_1 - \xi_j, x_2 - \eta_j) \ . \tag{1.87}$$

Algorithm 5 FMM on a level-restricted tree (evaluating the potential)

```
for all boxes B_{l,j} do
    if B_{l,j} is a leaf box then
        for all collocation points x_q do
            û(x_q) ← û(x_q) + local expansion due to b^{(l,j)} evaluated at x_q
            for all neighbors B_{l',j'} do
                û(x_q) ← û(x_q) + local interaction due to c^{(l',j')} using G^{B_{l',j'}}(x_q)
            end for
            for all boxes B_{l',j'} in the fine interaction list do
                û(x_q) ← û(x_q) + multipole expansion due to a^{l',j'} evaluated at x_q
            end for
        end for
    end if
end for
```

Also, let $Vf(\mathbf{x})$ denote the convolution (1.61) and $\tilde{V}f(\mathbf{x})$ denote the approximation computed via the FMM. If the FMM tolerance is set to ε (this is accomplished by taking p sufficiently large, typically $p \approx \log_2(1/\varepsilon)$), then

$$\begin{aligned}
\frac{|\hat{u}(\mathbf{x}_q) - u(\mathbf{x}_q)|}{\|\tilde{f}\|_\infty} &= \frac{\left|\tilde{V}\tilde{f}(\mathbf{x}_q) - V\tilde{f}(\mathbf{x}_q) + V\tilde{f}(\mathbf{x}_q) - Vf(\mathbf{x}_q)\right|}{\|\tilde{f}\|_\infty} \\
&\leq \varepsilon \frac{\|\tilde{f}\|_1}{\|\tilde{f}\|_\infty} + C(\Omega)\frac{\|f - \tilde{f}\|_\infty}{\|\tilde{f}\|_\infty} \\
&\leq \varepsilon|\Omega| + C(\Omega)\frac{\|f - \tilde{f}\|_\infty}{\|\tilde{f}\|_\infty} \,, \qquad (1.88)
\end{aligned}$$

where $|\Omega|$ denotes the area of the set Ω and

$$C(\Omega) = \frac{1}{2\pi}\max_{\mathbf{x}\in\Omega}\int_\Omega |\log\|\mathbf{x} - \mathbf{y}\||\, dy \,. \qquad (1.89)$$

This bound depends only on the values of the data f (as opposed to possibly high order derivatives of f), the precision of the FMM, and the accuracy of the

polynomial approximation. It is clear that for smooth f and uniform leaf boxes, this bound implies fourth order convergence up to the tolerance ε.

1.4.7 Error estimates for non-smooth densities

Let's perform a heuristic but more detailed analysis of the error bound (1.88) for densities f which are not necessarily smooth on the box Ω. Using the standard multi-index notation, let $\partial^{\boldsymbol{\alpha}} = \partial_{x_1}^{\alpha_1}\partial_{x_2}^{\alpha_2}$ and $|\boldsymbol{\alpha}| = \alpha_1 + \alpha_2$. Then the differentiability class $C^k(A)$ of a domain A is defined to be the set of functions g such that $\partial^{\boldsymbol{\alpha}} g$ is continuous for each $\boldsymbol{\alpha}$ with $|\boldsymbol{\alpha}| \leq k$, with the convention that $C^{-1}(A)$ is the set of bounded functions which are possibly discontinuous. For a density $f \in C^k(\Omega)$ and a uniform tree with leaf boxes of width h, let $\tilde{f}$ be the numerical approximation to f as above, using interpolants of order n (degree $n-1$) on each box. Standard error estimates imply that

$$\|f - \tilde{f}\|_\infty = \mathcal{O}(h^m)\,, \tag{1.90}$$

where $m = \min(k, n)$. If the additional assumption is made that f is piecewise C^{k+l} for some $l > 0$ (say that for a domain $A \subset \Omega$, the density $f \in C^{k+l}(A)$ and $f \in C^{k+l}(\Omega \setminus A)$) then theoretical results for one dimensional interpolation [47] suggest that it's reasonable to expect $m = \min(k+1, n)$, and this is what is seen in practice.

These bounds would suggest that the scheme should have $\mathcal{O}(1)$ error for a piecewise smooth density which is discontinuous across some boundary, but this is not the case. The bound (1.88) is too generous by using a constant determined by the L^1 norm of $G_L(\mathbf{x}, \mathbf{y}) = -\log\|\mathbf{x} - \mathbf{y}\|/2\pi$, but other norms are available. In

fact, if $G_L(\mathbf{x}, \cdot) \in L^r(\Omega)$ for all $\mathbf{x} \in \Omega$, then

$$\begin{aligned} |Vf(\mathbf{x}) - \tilde{V}\tilde{f}(\mathbf{x})| &\leq |V\tilde{f}(\mathbf{x}) - \tilde{V}\tilde{f}(\mathbf{x})| + |V(\tilde{f} - f)(\mathbf{x})| \\ &\leq \varepsilon \|\tilde{f}\|_1 + C(\Omega, r)\|\tilde{f} - f\|_q \,, \end{aligned} \tag{1.91}$$

where $1/r + 1/q = 1$ and the constant $C(\Omega, r)$ is given by

$$C(\Omega, r) = \max_{\mathbf{x} \in \Omega} \left(\int_\Omega |G_L(\mathbf{x}, \mathbf{y})|^r \, dy \right)^{1/r} .$$

In particular, the bound (1.91) holds with $r = 3/2$ for both the Green's function G_L and its first-order derivatives. Therefore, the order of accuracy of the scheme is bounded by the order of accuracy of $\|f - \tilde{f}\|_3$ up to the tolerance ε.

Using the bound (1.91) with $r = 3/2$, we can establish a higher order of accuracy for piecewise smooth densities f. For concreteness, let Ω be the unit box and f be piecewise smooth on a subdomain A and its complement $\Omega \setminus A$, with $f \in C^k(\Omega)$ globally. Consider a uniform tree on Ω with N leaf boxes Ω_i of width h (so that $N = 1/h^2$). Let $\mathcal{I} = \{i : \Omega_i \text{ intersects } \partial A\}$ be the set of indices of leaf boxes which intersect ∂A. Under mild assumptions on the boundary ∂A, the set $\mathcal{I}$ has $\mathcal{O}(1/h)$ indices. By construction, f is smooth for the $\mathcal{O}(1/h^2)$ leaf boxes Ω_i such that $i \notin \mathcal{I}$. If $m = \min(k + 1, n)$, then

$$\|f - \tilde{f}\|_3 \leq \sum_{i \notin \mathcal{I}} \|f - \tilde{f}\|_{L^3(\Omega_i)} + \sum_{i \in \mathcal{I}} \|f - \tilde{f}\|_{L^3(\Omega_i)} \tag{1.92}$$

$$\leq \sum_{i \notin \mathcal{I}} h^2 \|f - \tilde{f}\|_{L^\infty(\Omega_i)} + \sum_{i \in \mathcal{I}} h^2 \|f - \tilde{f}\|_{L^\infty(\Omega_i)} \tag{1.93}$$

$$= h^2(N - |\mathcal{I}|)\mathcal{O}(h^n) + h^2|\mathcal{I}|\mathcal{O}(h^m) \tag{1.94}$$

$$= \mathcal{O}(h^n) + \mathcal{O}(h^{m+1})\,. \tag{1.95}$$

In particular, the above implies that the error in the volume integral is $\mathcal{O}(h^{m'})$, where $m' = \min(k+2, n)$.

The above results show that the volume integral for a box code with a uniform tree and piecewise smooth density should converge with first order accuracy for globally discontinuous functions, with second order accuracy for globally continuous functions, and so on. We are interested in results for piecewise smooth functions which are globally C^k because we will eventually compute volume integrals using piecewise polynomial approximations of f, where we have used function extension to enforce global smoothness up to some order. Because the algorithm is adaptive, additional efficiencies can be achieved by using highly refined discretization along the user-specified boundary or in other regions where the local smoothness is not sufficient for the uniform order of accuracy estimates to apply.

From the inequality (1.92), it is clear that it's the smoothness of f on individual boxes which affects the pointwise error of the volume potential (1.91). However, the pointwise error is not the whole story for accuracy. Indeed, the potential Vf, in addition to the density f, should be resolved by its polynomial interpolants on the leaf boxes of the adaptive quad tree. If f is smooth and well resolved on the individual leaf boxes but discontinuous from box to box, then the potential Vf might not be well resolved on those same boxes. Therefore, the global smoothness of f, even as a function on $\mathbb{R}^2$, is of concern.

1.5 Summary and Discussion

In the previous sections, we have discussed the salient features of integral-equation methods, including the underlying theory for integral representations and fast solution methods. The methods are robust to perturbations in the solution and over-discretization of the domain. In many cases, the available tools have optimal computational complexity and straightforward error estimation. Integral-equation methods for inhomogeneous PDEs have also been shown to be amenable to modern computing environments, see, inter alia, [45, 46], and there is good reason to believe that such methods will be the basis of next-generation computational tools for simulation and design.

Chapter 2

Function extension via layer potentials

In the previous chapter, the groundwork was laid for using integral-equation methods to solve homogeneous boundary value problems in complex geometries and to solve inhomogeneous problems in free space with piecewise smooth data. These methods can be used together to obtain the solution of inhomogeneous problems in complex geometries, made especially efficient by using function extension. For the necessary volume integrals, we will rely on "box codes" as described in Section 1.4 together with error estimates discussed in Section 1.4.7. For the sake of simplicity, we limit our discussion to the Poisson equation. Other constant coefficient PDEs are handled in the analogous fashion. The rest of the chapter examines the problem of function extension, with a brief survey of existing schemes, a description of our new method for global function extension, and some details concerning the numerical implementation.

2.1 Integral equations for inhomogeneous PDEs

Let u be a solution to the Poisson equation with Dirichlet boundary conditions, i.e.

$$\Delta u = f \text{ in } \Omega \,, \tag{2.1}$$

$$u = g \text{ on } \partial\Omega \,, \tag{2.2}$$

for a density f and boundary data g.

As noted in the introduction, the standard potential theory-based approach to compute the solution of (2.1), (2.2) is based simply on the fact that the problem is linear. The first step is to calculate a particular solution, i.e. a function v which satisfies only the first condition (2.1). A natural candidate for v is given by

$$v(\mathbf{x}) = \int_\Omega G_L(\mathbf{x}, \mathbf{y}) f(\mathbf{y})\, dy, \tag{2.3}$$

where $G(\mathbf{x}, \mathbf{y})$ is the free-space Green's function for Poisson's equation. Once v has been computed, the second step is to compute a homogeneous solution with appropriate boundary conditions. In particular, one solves the following Dirichlet problem

$$\Delta u^H = 0 \text{ in } \Omega \tag{2.4}$$

$$u^H = g - v|_{\partial\Omega} \text{ on } \partial\Omega. \tag{2.5}$$

The solution to (2.1), (2.2) is then the sum $u = v + u^H$.

In the previous chapter, a box code was used to compute (2.3) in the case that Ω is a box. For a domain Ω which is not a box, a box code can still be used to obtain a particular solution. One simply chooses a box Ω_B such that $\Omega \subset \Omega_B$ and finds an extension f_e of the function f which is defined on Ω_B and satisfies $f_e|_\Omega = f$. Based on the analysis of Subsection 1.4.7, the extension f_e should ideally be as smooth as possible, both on leaf-boxes and as a function on $\mathbb{R}^2$. With such an extension, a particular solution is given by

$$v(\mathbf{x}) = \int_{\Omega_B} G_L(\mathbf{x}, \mathbf{y}) f_e(\mathbf{y})\, dy \,, \tag{2.6}$$

which can be computed using the method of the previous chapter.

We note that function extension, in this setting, is only necessary because the computational elements are regular in the box code and do not conform to the domain. For a discretization which conforms to the domain, say with cut cells, there is no need to extend the function beyond the domain. However, there are serious drawbacks to the use of cut cells (or any irregular computational elements) when evaluating (2.3). The corresponding FMM would not have the efficiencies available to a box code, which depend on the regularity of the grid. Further, the numerical quadrature for local interactions would be much more difficult as the interactions for the cut cells would have to be handled individually with computationally expensive adaptive quadrature.

2.2 Related ideas and existing work

The idea of using a code designed for regular domains to solve problems on a more geometrically complex domain has a long history in numerical methods. The immersed boundary method [54] was developed for fluid-structure interactions and treats a problem with a complex boundary by embedding it in a regular domain. The effect of the boundary is accounted for using mollified delta functions and the method was traditionally limited to low orders of accuracy. In the recent work [66], high order immersed boundary methods were presented which view the solution as a smooth function extended beyond the boundary of the domain. Indeed, the extended solution of [66] is viewed in much the same way as the extended density in the method presented below: as the solution of an appropriate polyharmonic equation. This results in an extended system for the solution in the regular domain, which includes unknown parameters to determine the nature of the extended solution.

Related to these ideas is the method of Mayo et al. [48], which also treats a domain with a complex boundary by embedding it in a regular domain. In this method, knowledge of the jumps in the solution across the boundary of the domain is used to modify a standard finite difference stencil so that higher orders of accuracy can be maintained. In the EBI method of [9, 10], the process of [48] was extended to fluids problems.

Because the above methods typically rely on a standard finite difference scheme, they are somewhat complicated to implement adaptively and still require non-trivial fast solvers. Box codes, on the other hand, are fast, adaptive and direct without the need to solve any linear system of equations.

In previous box code schemes for irregular domains, two techniques were used.

The first simply sets the density f_e to be zero outside the domain. In this case, the function f_e is as smooth as the original density f inside the domain and smooth outside the domain, as it is a constant. Therefore, the estimates for piecewise smooth functions apply and we see that the scheme should converge and is $\mathcal{O}(h)$ for a uniform tree with boxes of width h (again, the box code can be more efficient in terms of degrees of freedom than the uniform case by using an adaptive tree).

The second method uses local polynomial approximations to f to extrapolate f outside the domain over short distances (see [43]). This method results in a smooth f_e on each individual leaf box but has no guarantees of smoothness across boxes. Because there can be discontinuities in f_e near the original domain, the computed potential Vf_e has nearby singularities on those boxes. This issue seems to be unavoidable in local extrapolation methods and it is for this reason that we seek a global extrapolation method which increases the order of accuracy without excessive adaptive refinement.

2.3 A simple observation

The following is a simple method for computing a global extrapolation of the density f from its domain of definition Ω to Ω_B. Let w solve the PDE

$$\Delta w = 0 \quad \text{in } \mathbb{R}^2 \setminus \Omega\,, \tag{2.7}$$

$$w = f \quad \text{on } \partial\Omega\,, \tag{2.8}$$

subject to the condition that $w(\mathbf{x})$ is bounded as $\|\mathbf{x}\| \to \infty$. Then, the function f_e defined by

$$f_e(\mathbf{x}) = \begin{cases} f(\mathbf{x}) & \text{for} \quad \mathbf{x} \in \Omega \\ w(\mathbf{x}) & \text{for} \quad \mathbf{x} \in \Omega_B \setminus \Omega \end{cases} \tag{2.9}$$

is globally continuous, as smooth as f on Ω, and smooth on $\Omega_2 \setminus \Omega$. While this seems at first glance like a computationally expensive way to extrapolate f, the analytical and numerical machinery required to solve this problem is the same as that required to solve the harmonic problem (2.4), (2.5) which is used to enforce the boundary condition of the original Poisson problem (2.1), (2.2).

The method can also be generalized to compute globally C^k extrapolations of f by solving polyharmonic equations. For example, a C^1 extrapolation can be computed by solving the following biharmonic problem:

$$\Delta^2 w = 0 \quad \text{in } \mathbb{R}^2 \setminus \Omega\,, \tag{2.10}$$

$$w = f \quad \text{on } \partial\Omega\,, \tag{2.11}$$

$$\partial_\nu w = \partial_\nu f \quad \text{on } \partial\Omega\,, \tag{2.12}$$

with $|w(\mathbf{x})| = \mathcal{O}(|\mathbf{x}|^2)$ and $|\nabla w(\mathbf{x})| = \mathcal{O}(|\mathbf{x}|)$ as $|\mathbf{x}| \to \infty$. Once w is computed, f_e is defined as above. While the methods are not as well developed as in the Laplace case, there exist similar potential-theory based integral equations and fast solution methods for the biharmonic problem. See, for instance, the thesis [21] and the approach of [63] which leverages the Sherman-Lauricella integral equations for elasticity. There are two main reasons to avoid extrapolations using a polyharmonic

function of higher order than the biharmonic: (1) the requirement to provide high order derivatives of the data f at the boundary and (2) diminishing returns because of the power of adaptive refinement.

We also note the following possibility for the extension of a divergence-free vector field. Let $\mathbf{b}$ be a divergence-free field on Ω. Then, if $\mathbf{w}$ is a solution of

$$\begin{aligned} \alpha^2\mathbf{w} - \Delta\mathbf{w} &= -\nabla p \quad \text{in } \Omega_2 \setminus \Omega\,, && (2.13)\\ \nabla\cdot\mathbf{w} &= 0 \quad \text{in } \Omega_2 \setminus \Omega\,, && (2.14)\\ \mathbf{w} &= \mathbf{b} \quad \text{on } \partial\Omega \cap \partial\Omega_2\,, && (2.15)\\ \mathbf{w} &= \mathbf{0} \quad \text{on } \partial\Omega_2 \setminus \partial\Omega\,, && (2.16) \end{aligned}$$

we can use $\mathbf{w}$ to define an extension $\mathbf{b}_e$ as above which is globally continuous and divergence-free on the sets Ω and $\Omega_2 \setminus \Omega$. Tools for computing $\mathbf{w}$ are presented in Chapter 4.

2.4 Convergence rates

We investigate the effect of function extension on the observed convergence rate of a box code in a simple setting. Let Ω be the unit disc and Ω_B be the box $[-2,2]\times[-2,2]$. We consider the Poisson problem for an exact solution $u(\mathbf{x}) = x_1^2/2 + x_1 + x_2 + 5$, for which the right hand side f is the constant 1. We extend f beyond the disc in three ways: (1) extension by zero, (2) continuous (but not C^1) extension, and (3) smooth extension. Such extensions are easy to obtain by setting $f_e = 0$, $f_e = \sqrt{x_1^2+x_2^2}(1-\log\sqrt{x_1^2+x_2^2})$, and $f_e = 1$ outside the domain,

respectively.

We enforce the boundary conditions by solving the appropriate homogeneous problem using a double layer potential formulation. In Table 2.1, we report the maximum error E_i of the results computed with these extension methods for a given number number of grid points N_i arranged in a uniform tree. We see that the continuous extension outperforms the extension by zero dramatically, in terms of accuracy and convergence rate. The observed convergence rate is actually a little faster than the first order convergence (for extension by zero) and second order convergence (for continuous extension) predicted by the bounds of the previous chapter. For the smooth extension, high accuracy and fourth order convergence are observed, as expected.

	Zero extension		Continuous extension		Smooth extension	
N_i	E_i	E_i/E_{i+1}	E_i	E_i/E_{i+1}	E_i	E_i/E_{i+1}
$16 \cdot 4$	2.535E-004	6.650	3.128E-006	10.27	4.267E-006	13.25
$16 \cdot 4^2$	3.812E-005	4.150	3.045E-007	6.037	3.218E-007	15.02
$16 \cdot 4^3$	9.185E-006	3.499	5.045E-008	26.79	2.142E-008	15.58
$16 \cdot 4^4$	2.624E-006	3.562	1.883E-009	7.550	1.375E-009	15.53
$16 \cdot 4^5$	7.367E-007	3.463	2.494E-010	16.13	8.848E-011	11.40
$16 \cdot 4^6$	2.127E-007	N/A	1.545E-011	N/A	7.759E-012	N/A

Table 2.1: Convergence rates for extension by zero, continuous extension, and smooth extension.

2.5 Numerical implementation of continuous extension

The integral-equation methods used to compute the continuous extension via (2.7), (2.8) are largely standard. In this section, we present the representation for the extension, the corresponding integral equation, and a new method used to

evaluate the extension at arbitrary points of $\Omega_B \setminus \Omega$. In the following, we assume that Ω is simply connected but the ideas apply to multiply connected domains in a straightforward manner.

2.5.1 Layer potential representation of the extension

We represent w as a double layer potential, as defined in (1.41), in the exterior of Ω, i.e. we set $w = D\mu$ for an unknown density μ given on $\partial\Omega$. It is well known that the double layer potential cannot represent all bounded harmonic potentials in an exterior domain (as it necessarily decays) but the representation can be made complete by adding a constant term. We set $w = (D + W)\mu$ where

$$W\mu(\mathbf{x}) = \int_{\partial\Omega} \mu(\mathbf{y})\, dS(\mathbf{y}) \,. \tag{2.17}$$

2.5.2 Boundary integral equation

Using the jump conditions (1.43), we find that the boundary conditions for w impose the following integral equation

$$\frac{1}{2}\mu(\mathbf{x}_0) + \mathcal{D}\mu(\mathbf{x}_0) + \mathcal{W}\mu(\mathbf{x}_0) = f \,, \tag{2.18}$$

where $\mathcal{W}$ is the operator W restricted to the boundary and $\mathbf{x}_0$ is on the boundary $\partial\Omega$. This is a second-kind integral equation and the Fredholm alternative applies. The invertibility of this equation follows standard arguments. In [28], a proof of existence-uniqueness is worked out for the three dimensional analogue of this problem.

For the case of a smooth domain, the discretization of this integral equation

is particularly simple, as the integral kernel has a removable singularity. We use the Nyström method with panels of scaled Legendre nodes and standard Gaussian quadrature weights. In order to compute the solution of the resulting linear system, we use the fast direct solver of [31].

2.5.3 Layer potential evaluation with quadrature by expansion

While a standard solution procedure can be used to compute the density corresponding to the extension, the requirements for evaluating the layer potential can be somewhat non-standard. This is because, in an adaptive setting, the grid points at which the values of the layer potential are desired may not be known a priori. Therefore, we have developed a variant of QBX (quadrature by expansion), which performs a precomputation and then allows for $\mathcal{O}(1)$ access to the values of the potential at arbitrary locations.

2.5.3.1 QBX and the FMM

In order to obtain a fast implementation of QBX, we couple it to the FMM. There are many options for doing this and we present a simple one here. For a method which makes fewer assumptions about the discretization of the boundary, see [62].

For concreteness, we consider the use of QBX to evaluate a single layer potential $u = S\sigma$ for a curve Γ, where S is as defined in (1.37). Let $\mathbf{c}$ be a QBX center located at a distance r from the boundary. In the QBX method, the potential u is approximated by a power series in the disc $B_r(\mathbf{c})$, i.e.

$$u(\mathbf{x}) = \mathrm{Re}\left(\sum_{l=0}^{p} \alpha_l (z-\xi)^l\right) , \tag{2.19}$$

where $\mathbf{x}$ is in $B_r(\mathbf{c})$, $z = x_1 + ix_2$, and $\xi = c_1 + ic_2$. Using standard separation of variables on the circle of radius $r/2$ about $\mathbf{c}$, we have

$$\alpha_l = \frac{2^l}{2\pi r^l} \int_0^{2\pi} u\left(\mathbf{c} + \frac{r}{2}\begin{pmatrix}\cos\theta \\ \sin\theta\end{pmatrix}\right) e^{-il\theta}\, d\theta\,. \tag{2.20}$$

To compute the α_l numerically, let Γ be discretized into panels with q scaled Legendre nodes on each. For simplicity, we assume that the panels are all of the same length h. We also assume that $\overline{B_r(\mathbf{c})}$ intersects Γ for at most one point. Then, the bounds for the quadrature error for computing u on $\partial B_{r/2}(\mathbf{c})$ are of the same form as the estimates in [18]. Let $\hat{u}(\mathbf{y})$ be the computed value of u using the smooth Gaussian quadrature rule for each panel. If σ is in the Hölder space $C^{p,\beta}(\Gamma) \cap C^{2q,\beta}(\Gamma)$, then there exists a constant $\overline{C}_{q,\beta}$ such that

$$|\hat{u}(\mathbf{y}) - u(\mathbf{y})| \leq \left(\frac{h}{2r}\right)^{2q} \|\sigma\|_{C^{2q,\beta}(\Gamma)} , \tag{2.21}$$

for $\mathbf{y}$ on $\partial B_{r/2}(\mathbf{c})$. We can then evaluate $\hat{u}$ for M_{QBX} equispaced points on the circle $\partial B_{r/2}(\mathbf{c})$ and use the trapezoidal rule to compute the α_l as in (2.20), with exponential convergence in M_{QBX}. For sufficient sampling, M_{QBX} should be taken larger than $2p$.

Using this procedure for computing the coefficients α_l, it is clear how to accelerate QBX with the FMM. Let the boundary nodes be given by $\mathbf{x}_i$ and the smooth Gaussian weights by w_i. Then, the M_{QBX} values for each expansion center can be computed with a standard FMM call, with point charges of strength $\sigma(\mathbf{x}_i)w_i$ at

each boundary node $\mathbf{x}_i$ (often, the boundary points are over-sampled to increase the accuracy of the computed coefficients).

2.5.3.2 Evaluating layer potentials at arbitrary locations in constant time

Suppose first that we would like to evaluate the single layer potential $u = S\sigma$ at a set of target points $\mathbf{t}_i$ for $i = 1, \ldots, M_t$, which can be close to the boundary Γ. Let Γ be discretized as in the previous section, with N points $\mathbf{x}_i$ and weights w_i. Denote the outward normal to the boundary at the point $\mathbf{x}$ by $\boldsymbol{\nu}(\mathbf{x})$. Then, the following steps compute the potential at each target using the QBX rule for near-boundary targets.

- Place N QBX centers at the points $\mathbf{c}_i = \mathbf{x}_i - h\boldsymbol{\nu}(\mathbf{x}_i)$.
- Define M_{QBX} equispaced points $\mathbf{y}_{i,j}$ for $j = 1, \ldots, M_{QBX}$ on the circle of radius $h/2$ about each center $\mathbf{c}_i$.
- Call the FMM with charges of strength $\sigma(\mathbf{x}_i)w_i$ located at the boundary points and targets given by the union of the $\mathbf{t}_i$ and the $\mathbf{y}_{i,j}$. This is a $\mathcal{O}(NM_{QBX} + M_t)$ procedure.
- Compute the coefficients α_l for each center as in (2.20), using the trapezoidal rule. This takes $\mathcal{O}(NM_{QBX} \log M_{QBX})$ work for $M_{QBX} > p$ using the FFT.
- For each target which is within $h/2$ of the boundary, let $\mathbf{c}_i$ be the nearest QBX center. The smooth rule might not be accurate for this target, so instead use the value given by the power series about $\mathbf{c}_i$ as in (2.19). The cost for this is $\mathcal{O}(p)$ per target.

Suppose now that the above steps have been completed and that we would like to evaluate the potential for a new target $\mathbf{t}$. If the target is near to the boundary, the potential can be computed using the expansion about the nearest QBX center. However, if the target is further from the boundary it seems that the FMM would need to be called again to compute the potential. It is easy, however, to modify the FMM so that it only needs to be called once.

In the following, we use the notation of Section 1.4 for the FMM. Suppose that the target $\mathbf{t}$ is contained in the leaf box Ω_i of the FMM hierarchy. For Ω_i, we denote the set of neighbors by

$$\mathcal{N}(i) = \{j : \Omega_j \text{ is a neighbor of } \Omega_i\} \tag{2.22}$$

and the fine interaction list by

$$\mathcal{F}(i) = \{j : \Omega_j \text{ is in the fine interaction list of } \Omega_i\} \ . \tag{2.23}$$

The value of the potential at the target $\mathbf{t}$ is computed as the sum

$$\begin{aligned} \hat{u}(\mathbf{t}) &= -\frac{1}{2\pi} \sum_{j \in \mathcal{N}(i)} \sum_{k : \mathbf{x}_k \in \Omega_j} \log \|\mathbf{t} - \mathbf{x}_k\| \sigma(\mathbf{x}_k) w_k \\ &\quad + \sum_{j \in \mathcal{F}(i)} \phi_{\Omega_j}(\mathbf{t}) + \Psi_{\Omega_i}(\mathbf{t}) \ , \end{aligned} \tag{2.24}$$

where ϕ_{Ω_j} is the multipole expansion due to the charges in a box and Ψ_{Ω_i} is the local expansion. We note that typically there will not be any boundary points in the neighbor boxes for such a target so that the first part of the sum (2.24) is zero.

In a single call to the FMM, the multipole and local expansion coefficients can be computed for all boxes in the hierarchy. Therefore, if these coefficients are

stored for the initial call to the FMM, the value at a new target $\mathbf{t}$ can be evaluated in $\mathcal{O}(p_{FMM})$ work, where p_{FMM} is the order of the multipole and local expansions in the FMM.

Chapter 3

On-the-fly quadrature for the Yukawa potential

As noted in Chapter 1, the solution to the Yukawa problem (or the modified Helmholtz problem) in free-space is given by convolution with the fundamental solution. If f is smooth and compactly supported, then

$$u(\mathbf{x}) = \frac{1}{2\pi} \int_{\mathbb{R}^2} K_0(\lambda \|\mathbf{x} - \mathbf{y}\|) f(\mathbf{y})\, dy \,, \tag{3.1}$$

where K_0 is the modified Bessel function of the second kind, solves

$$-\Delta u + \lambda^2 u = f \,, \tag{3.2}$$

with $u(\mathbf{x}) \to 0$ as $\|\mathbf{x}\| \to \infty$.

In Section 1.4, we outlined a particularly efficient fast multipole method, based on [19], for computing a similar convolution in the case of the Poisson equation. We refer to such schemes as "box codes" and note that, in terms of the integral kernel,

their speed depends on the ability to manipulate multipole and local expansions to evaluate the far field and the ability to infer local interaction tables based on a few precomputed values (as the name implies, much of the efficiency is due to the way the domain and density f are discretized). The authors of [13] described and implemented a box code for the Yukawa equation, following the presentation of [19]. For the simulations in this thesis, we use the FMM adapted to the Yukawa potential as in [13] but with a new approach to the local interaction tables.

In Section 3.1, we discuss some of the salient features of the method presented in [13], with a focus on the differences between a box code for the Yukawa equation and one for the Poisson equation. We explain that the approach to generating local interaction tables of [13], which is very fast and largely based on precomputation, has some downsides and argue for an on-the-fly approach to table generation. Such an approach is described in Section 3.2 and should be of interest in more general settings.

3.1 A Yukawa box code

The box code for computing (3.1) differs from the one presented in Section 1.4 primarily in terms of the functions used for the multipole and local expansions of the potential. We present the relevant theorems from [13].

Theorem 3.1. *(Graf's addition theorem, see [17] section 10.23.) Assume the polar coordinates for the points* $\mathbf{x} = (x_1, x_2)$ *and* $\mathbf{y} = (y_1, y_2)$ *are given by* (ρ_x, θ_x) *and* (ρ_y, θ_y)*, respectively. If* $\rho_x > \rho_y$*, then*

$$K_0(\lambda\|\mathbf{x}-\mathbf{y}\|) = \sum_{l=-\infty}^{\infty} K_l(\lambda\rho_x) I_l(\lambda\rho_y) e^{il(\theta_x-\theta_y)} \,, \tag{3.3}$$

where I_l and K_l are the modified Bessel functions of order l of the first and second kind, respectively.

With the above theorem it is clear how to form the multipole coefficients as in (1.69), (1.71). Instead of integrating the density against z^l, one integrates against $I_l(\lambda\rho)e^{il\theta}$. We note that the scaling is not as simple as in the Poisson case and that the map from the coefficients of the density to the multipole coefficients must be computed for each level of the tree, rather than once.

The translation of a multipole expansion and the conversion of a multipole expansion into a local expansion are also based on Graf's addition theorem. We have

Theorem 3.2. *(Adapted from [13].) Suppose that*

$$\phi(\mathbf{x}) = \sum_{l=-\infty}^{\infty} a_l K_l(\lambda\rho')e^{il\theta'} \ , \tag{3.4}$$

where (ρ', θ') are the polar coordinates of $\mathbf{x}$ with respect to the point $\mathbf{x}_0$, is a multipole expansion of the potential due to a charge density which is contained inside the disc of radius R about $\mathbf{x}_0$. Let (ρ_0, θ_0) be the polar coordinates of $\mathbf{x}_0$ with respect to the origin. Then, for $\mathbf{x}$ outside the disc of radius $R + \rho_0$, we have

$$\phi(\mathbf{x}) = \sum_{l=-\infty}^{\infty} b_l K_l(\lambda\rho)e^{il\theta} \ , \tag{3.5}$$

where (ρ, θ) are the coordinates of $\mathbf{x}$ with respect to the origin and the translated coefficients are given by

$$b_l = \sum_{m=-\infty}^{\infty} a_m I_{l-m}(\lambda\rho_0)e^{-i(l-m)\theta_0} \ . \tag{3.6}$$

Theorem 3.3. *(Adapted from [13].) Suppose that*

$$\phi(\mathbf{x}) = \sum_{l=-\infty}^{\infty} a_l K_l(\lambda\rho')e^{il\theta'} , \tag{3.7}$$

where (ρ', θ') *are the polar coordinates of* $\mathbf{x}$ *with respect to the point* $\mathbf{x}_0$*, is a multipole expansion of the potential due to a charge density which is contained inside the disc of radius* $R < |\mathbf{x}_0|$ *about* $\mathbf{x}_0$*. Let* (ρ_0, θ_0) *be the polar coordinates of* $\mathbf{x}_0$ *with respect to the origin. Then, for* $\mathbf{x}$ *within the disc of radius* $\rho_0 - R$*, we have*

$$\phi(\mathbf{x}) = \sum_{l=-\infty}^{\infty} b_l I_l(\lambda\rho)e^{il\theta} , \tag{3.8}$$

where (ρ, θ) *are the coordinates of* $\mathbf{x}$ *with respect to the origin and the translated coefficients are given by*

$$b_l = \sum_{m=-\infty}^{\infty} a_m(-1)^m K_{l-m}(\lambda\rho_0)e^{-i(l-m)\theta_0} . \tag{3.9}$$

As in the FMM for the Poisson kernel, computing the multipole to local translations is one of the most expensive steps. This can be sped up by representing the multipole expansions by equivalent plane-wave expansions, which can be translated using $\mathcal{O}(p)$ operations for an expansion of length p. Again, the details are somewhat technical and we refer the interested reader to [13, 33].

The translation of local expansions is based on the following theorem.

Theorem 3.4. *(Adapted from [13].) Suppose that*

$$\Psi(\mathbf{x}) = \sum_{l=-\infty}^{\infty} a_l I_l(\lambda\rho)e^{il\theta} , \tag{3.10}$$

where (ρ, θ) *are the polar coordinates of* $\mathbf{x}$ *with respect to the origin, is a local ex-*

pansion for a parent box centered at the origin. Let (ρ_0, θ_0) *be the polar coordinates of the center* $\mathbf{x}_0$ *of a child box with respect to the origin. Then, for* $\mathbf{x}$ *inside the child box, we have*

$$\Psi(\mathbf{x}) = \sum_{l=-\infty}^{\infty} b_l I_l(\lambda\rho') e^{il\theta'} \ , \tag{3.11}$$

where (ρ', θ') *are the coordinates of* $\mathbf{x}$ *with respect to the child's center* $\mathbf{x}_0$ *and the new local expansion coefficients are given by*

$$b_l = \sum_{m=-\infty}^{\infty} a_m I_{l-m}(\lambda\rho_0) e^{-i(l-m)\theta_0} \ . \tag{3.12}$$

Using the above theorems, the far field interactions can be carried out as in Section 1.4. We would like to use precomputed tables of values for the local interactions, as we did for the Poisson kernel. For a leaf box B with center $\mathbf{x}_B = (\xi, \eta)$, let $\mathbf{f}$ denote the values of the density on the 4×4 grid of collocation points on B. We map these values to coefficients c_k of the 10 polynomials p_k as before. Let B' be a neighbor box of B and $\mathbf{x}_q$ a collocation point on B'. If ϕ_B is the potential due to the density f restricted to B, then we have

$$\begin{aligned}
\phi_B(\mathbf{x}_q) &= \frac{1}{2\pi} \int_B K_0(\lambda \|\mathbf{x}_q - \mathbf{y}\|) f(\mathbf{y})\, dy & (3.13)\\
&\approx \frac{1}{2\pi} \sum_{k=1}^{10} c_k \int_B K_0(\lambda \|\mathbf{x}_q - \mathbf{y}\| p_k(y_1 - \xi, y_2 - \eta)\, dy & (3.14)\\
&= \sum_{k=1}^{10} c_k G_k^B(\mathbf{x}_q; \lambda) \ . & (3.15)
\end{aligned}$$

Let D denote the unit box centered at the origin and let h be the side length of

B. Then

$$
\begin{aligned}
G_k^B(\mathbf{x}_q;\lambda) &= \frac{1}{2\pi}\int_B K_0(\lambda\|\mathbf{x}_q-\mathbf{y}\|p_k(y_1-\xi,y_2-\eta)\,dy && (3.16)\\
&= \frac{h^{m(k)+2}}{2\pi}\int_D K_0(\lambda h\|(\mathbf{x}_q-\mathbf{x}_B)/h-\mathbf{y}\|p_k(y_1,y_2)\,dy && (3.17)\\
&= h^{m(k)+2}G_k^D((\mathbf{x}_q-\mathbf{x}_B)/h;\lambda h)\ , && (3.18)
\end{aligned}
$$

where $m(k)$ is the total degree of p_k. We see that the local interaction tables must be computed for each possible box size h in the tree hierarchy, i.e. we require a distinct set of interaction tables for each level of the tree.

In [13], the computation of the local interaction tables is based on the observation that the entries in these tables are smooth functions of the parameter $\tilde{\lambda} = \lambda h$. Therefore, the tables are precomputed for a large number of values of $\tilde{\lambda}$, taken as scaled Legendre nodes on intervals of the real line. The table for a given $\tilde{\lambda}$ is then interpolated from these values. This is a fast process once the precomputation has been performed (and the result can even be stored in a file) but the storage requirements are quite large and seem unfavorable for a modern distributed computing environment. Further, for complex values of the parameter, including the Helmholtz equation, or for local interactions in three dimensions, the storage requirements would be even greater.

3.2 On-the-fly computation

3.2.1 Tables via multipoles

We develop here an on-the-fly approach to building local interaction tables. Let D be the unit box centered at the origin. Suppose that D is divided into 64 equal size boxes, as in Figure 3.2.1. Note that each of the collocation points of the colleague box is well-separated from all 64 of the smaller boxes. Further, each collocation point of D is well-separated from all but 4 of the smaller boxes.

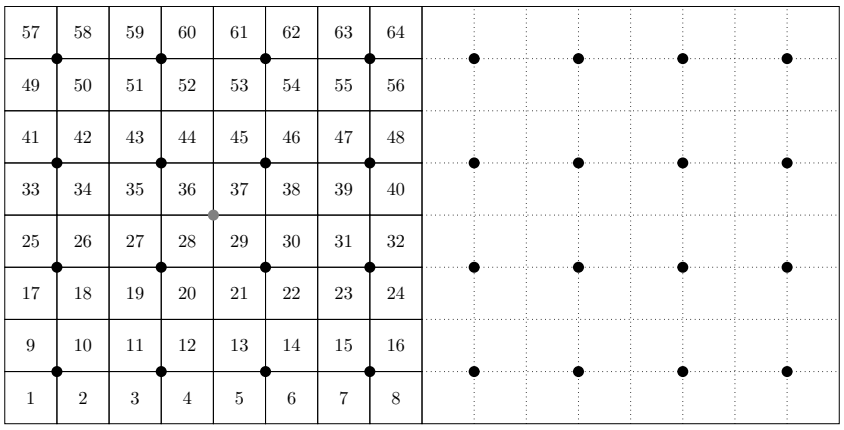

Figure 3.1: The unit box and a colleague. The collocation points are denoted by black dots and the origin is denoted by a gray dot.

To compute the values of $G_k^D(\mathbf{x}_q;\tilde{\lambda})$ for a given $\tilde{\lambda}$, we begin by forming the multipole expansions due to the polynomial p_k restricted to each of the 64 smaller boxes. For each of the collocation points $\mathbf{x}_q$ on the colleagues of D, the values of $G_k^D(\mathbf{x}_q;\tilde{\lambda})$ can then be computed simply by evaluating the sum of these 64 multipole expansions (the same is true of the collocation points on a neighbor box at a coarser discretization level). For collocation points on fine neighbors of D, we note that all but 4 of the collocation points are well-separated from all 64 smaller boxes, so the same procedure can be used for these. The remaining points can be

handled by dividing the boxes along the border of D each into 4 smaller boxes and then using a similar approach.

Of course, there is a lot of symmetry in these tables which can be exploited. In particular, many of the colleague, fine neighbor, and coarse neighbor interactions can be determined given the values for only a subset of these interactions. Using symmetry in this way results in significant speed-up. Much of the above can also be accelerated by using a hierarchical strategy in the spirit of the FMM. We found that this was largely unnecessary in two dimensions, as the speed of the brute force computation was acceptable, but this may be of use in three dimensions and for higher order interpolation nodes. Finally, we note that the interaction tables for derivatives of the kernels can be computed for these points by taking derivatives of the multipole expansions.

3.2.2 Self interactions

To finish the computation for the collocation points on D itself, we note that what remains is the influence of the 4 nearest small boxes for each of the collocation points. By rescaling, this interaction is given by a linear combination of the values of

$$\frac{1}{2\pi} \int_D K_0(\lambda' \|\mathbf{y}\|) p_k(y_1, y_2)\, dy \ , \tag{3.19}$$

for $k = 1, \ldots, 10$ and $\lambda' = \tilde{\lambda}/4$. We present a hybrid approach to computing these values, with different techniques for different regimes of the parameter λ'.

For $0 < \lambda' < 1$ and $r < 1$, the power series

$$K_n(\lambda' r) = \frac{2^{n-1}}{(\lambda' r)^n} \sum_{k=0}^{n-1} \frac{(n-k-1)!}{k!} (-1)^k \left(\frac{\lambda' r}{2}\right)^{2k} + (-1)^{n+1} \log\left(\frac{\lambda' r}{2}\right) I_n(\lambda' r) + (-1)^n \frac{(\lambda' r)^n}{2^{n+1}} \sum_{k=0}^{\infty} (\psi(k+1) + \psi(n+k+1)) \frac{\left(\frac{\lambda' r}{2}\right)^{2k}}{k!(n+k)!} , \tag{3.20}$$

where ψ denotes the digamma function, converges rapidly. The I_n also have a rapidly convergent power series given by

$$I_n(\lambda' r) = \left(\frac{\lambda' r}{2}\right)^n \sum_{k=0}^{\infty} \frac{\left(\frac{\lambda' r}{2}\right)^{2k}}{k!(n+k)!} . \tag{3.21}$$

For reference, see chapter 10 of [17]. We can then use a few terms of the power series for K_0 to approximate K_0 to high accuracy. The terms in the power series of K_0 are of the form $(\lambda' r)^{2k} \log(\lambda' r)$ and $(\lambda' r)^{2k}$. For $r = \|\mathbf{y}\|$ these terms are polynomials or a logarithm times a polynomial. We have the following analytical formulas for integrals of functions of this form.

Lemma 3.5. *Let $p(y_1, y_2) = y_1^{m_1} y_2^{m_2}$, for integers m_1 and m_2. If either m_1 or m_2 is odd, then*

$$\int_D p(y_1, y_2)\, dy = 0 \tag{3.22}$$

$$\int_D \log(x^2 + y^2) p(y_1, y_2)\, dy = 0 . \tag{3.23}$$

If $m_1 = 2l_1$ and $m_2 = 2l_2$, then

$$\int_D p(y_1, y_2)\, dy = \frac{1}{(m_1+1)(m_2+1)2^{m_1+n_1}} , \tag{3.24}$$

$$\int_D \log(y_1^2 + y_2^2) p(y_1, y_2)\, dy = \frac{a(l_1, l_2) + b(l_1, l_2) + c(l_1, l_2)}{d(l_1, l_2)} , \tag{3.25}$$

where

$$
\begin{aligned}
a(l_1,l_2) &= \frac{1}{4}(2l_1+1)\left(\psi\left(\tfrac{3}{4}+\tfrac{l_2}{2}\right)-\psi\left(\tfrac{1}{4}+\tfrac{l_2}{2}\right)\right)\ , && (3.26)\\
b(l_1,l_2) &= \frac{1}{4}(2l_2+1)\left(\psi\left(\tfrac{3}{4}+\tfrac{l_1}{2}\right)-\psi\left(\tfrac{1}{4}+\tfrac{l_1}{2}\right)\right)\ , && (3.27)\\
c(l_1,l_2) &= -(1+l_1+l_2)\log 2-\frac{2l_1+1}{2l_2+1}-\frac{2l_2+1}{2l_1+1}-1\ , && (3.28)\\
d(l_1,l_2) &= (1+l_1+l_2)(2l_1+1)(2l_2+1)2^{2l_1+2l_2}\ . && (3.29)
\end{aligned}
$$

With the above formulas, the integrals of the form (3.19) can be computed rapidly for $0 < \lambda' < 1$. We can take a similar semi-analytic approach for large values of λ'. The function $K_0(\lambda' r)$ decays exponentially in $\lambda' r$. For large values of λ', say $\lambda' > 4096$, the function $K_0(\lambda'\|\mathbf{y}\|)$ is zero to high precision outside of the unit box, i.e.

$$
\frac{1}{2\pi}\int_D K_0(\lambda'\|\mathbf{y}\|)p_k(y_1,y_2)\,dy \approx \frac{1}{2\pi}\int_{\mathbb{R}^2} K_0(\lambda'\|\mathbf{y}\|)p_k(y_1,y_2)\,dy \qquad (3.30)
$$

is an accurate approximation. There are analytical formulas for the latter integral. We have (see section 10.43 of [17])

Lemma 3.6. *Let $\lambda' > 0$. Then*

$$
\begin{aligned}
\int_{\mathbb{R}^2} K_0(\lambda'\|\mathbf{y}\|)\,dy &= \frac{2\pi}{(\lambda')^2}\ , && (3.31)\\
\int_{\mathbb{R}^2} K_0(\lambda'\|\mathbf{y}\|)y_1^2y_2^2\,dy &= \frac{4\pi}{(\lambda')^4}\ . && (3.32)
\end{aligned}
$$

For $p_k(y_1, y_2) = y_1^{m_1} y_2^{m_2}$ such that either $m_1 = 0$ or $m_2 = 0$, we have

$$\int_{\mathbb{R}^2} K_0(\lambda' \|\mathbf{y}\|) p_k(y_1, y_2)\, dy = 0\ . \tag{3.33}$$

At first, the requirement that $\lambda' > 4096$ would seem to be rather extreme, given that $K_0(35)$ is about machine epsilon for double precision arithmetic. However, we want good *relative* precision for the approximation (3.30), which requires a larger lower bound for λ'.

In the middle range, $1 < \lambda' \leq 4096$, we use an interpolation approach as in [13], but the storage requirements have been greatly reduced.

3.2.3 Derivatives of self interactions

The derivatives of the contribution to the potential of the form (3.19) can be computed using integration by parts. We demonstrate the procedure with an example. Consider integrals of the form

$$\frac{1}{2\pi} \int_D \left(\partial_{y_1} K_0(\lambda' \|\mathbf{y}\|)\right) p(y_1, y_2)\, dy\ , \tag{3.34}$$

where $p(y_1, y_2) = y_1^{m_1} y_2^{m_2}$ for integers m_1 and m_2. Generally, the integrand is weakly singular on D, so that the value exists as an improper integral. The integral is non-zero for m_1 odd and m_2 even, while other values of m_1 and m_2 give zero by symmetry. For m_1 odd and m_2 even, the function $K_0(\lambda' \|\mathbf{y}\|) y_1^{m_1} y_2^{m_2}$ is even with respect to y_1 and y_2. We use this fact and standard to integration by parts to obtain:

$$4\int_D (\partial_{y_1} K_0(\lambda'\|\mathbf{y}\|)) y_1^{m_1} y_2^{m_2}\, dy \tag{3.35}$$

$$= \int_0^{1/2}\int_0^{1/2} (\partial_{y_1} K_0(\lambda'\|\mathbf{y}\|))\, y_1^{m_1} y_2^{m_2}\, dy_1\, dy_2$$

$$= \frac{1}{2^{m_1}} \int_0^{1/2} K_0(\lambda'\sqrt{1/4+y_2^2}))y_2^{m_2}\, dy_2$$

$$- m_1 \int_0^{1/2}\int_0^{1/2} K_0(\lambda'\|\mathbf{y}\|) y_1^{m_1-1} y_2^{m_2}\, dy_1 dy_2\ , \tag{3.36}$$

where the integrals in the above are interpreted as improper integrals. The first term in the resulting expression is a one dimensional integral with a smooth integrand. This can therefore be computed rapidly and accurately using a high order smooth quadrature rule. For the second term, we can use the techniques outlined in the previous subsection.

Interestingly, the approach taken above also works for second derivatives of the self interaction. Consider integrals of the form

$$\frac{1}{2\pi} \oint_D \left(\partial_{y_i y_j} K_0(\lambda'\|\mathbf{y}\|)\right) p(y_1, y_2)\, dy\ , \tag{3.37}$$

where $i, j \in \{1, 2\}$ and the symbol $\oint$ indicates that the integral is to be interpreted in the Cauchy principal value sense. The integrand may be singular in general, though this is only the case for constant p.

Let $p \equiv 1$. Then we have

$$\frac{1}{2\pi} \oint_D (\partial_{y_1 y_2} K_0(\lambda'\|\mathbf{y}\|))\, p(y_1, y_2)\, dy = 0\ , \tag{3.38}$$

because the integrand is odd (in both y_1 and y_2). Further, we have that

$$\frac{1}{2\pi}\oint_D \left(\partial_{y_1 y_1} K_0(\lambda'\|\mathbf{y}\|)\right) p(y_1, y_2)\, dy = \frac{1}{2\pi}\oint_D \left(\partial_{y_2 y_2} K_0(\lambda'\|\mathbf{y}\|)\right) p(y_1, y_2)\, dy\ . \quad (3.39)$$

Then, we can use that $-(\Delta - \lambda'^2)K_0(\lambda'\|\mathbf{x}-\mathbf{y}\|) = \delta(\mathbf{x}-\mathbf{y})$ to obtain

$$\frac{1}{2\pi}\oint_D \left(\partial_{y_1 y_1} K_0(\lambda'\|\mathbf{y}\|)\right) p(y_1, y_2)\, dy = -\frac{1}{4\pi} + \frac{\lambda'^2}{2\pi}\int_D K_0(\lambda'\|\mathbf{y}\|)\, dy\ . \quad (3.40)$$

For p of higher degree, the integrand is weakly singular and the integrals can be interpreted as improper integrals. The same integration by parts technique as was used for the first order derivatives can be applied in most cases, except in the case that $m_1 = 0$ and both derivatives are with respect to y_2 (or vice versa). However, this case can be handled using the delta function trick as above.

Chapter 4

A stabilized FMM for the integral equations of unsteady flow

The boundary conditions in a semi-implicit method for the Navier-Stokes equations can be imposed by solving the modified Stokes equations at each time step. For reference, the modified Stokes equations with zero forcing in a domain Ω with boundary Γ are:

$$\begin{aligned} \Delta \mathbf{u} - \alpha^2 \mathbf{u} &= \nabla p \quad \text{in } \Omega \,, & (4.1) \\ \mathbf{u} &= \mathbf{g} \quad \text{on } \Gamma \,, & (4.2) \\ \nabla \cdot \mathbf{u} &= 0 \,, & (4.3) \end{aligned}$$

where $\mathbf{u}$ is the velocity and p is the pressure. Because of the divergence-free condition, the boundary data $\mathbf{g}$ must satisfy the compatibility criterion

$$\int_\Gamma \mathbf{g} \cdot \mathbf{n}\, dS = 0\ . \tag{4.4}$$

In the context of time stepping for Navier-Stokes, the parameter α will be given by an expression like $\sqrt{Re/\delta t}$, where Re is the Reynolds number and δt is the length of the current time step.

In this chapter, we discuss some of the analytical and algorithmic aspects of solving the modified Stokes equations using integral-equation methods. Section 4.1 contains a brief review of the relevant literature, beginning with methods for the Stokes equations (the $\alpha = 0$ case). We use the completed double layer method for our calculations, so this formulation is discussed in some detail.

The completed double layer method makes use of the Green's function for the modified biharmonic problem, which requires some care in a fast multipole method framework. In particular, a naïve implementation would result in catastrophic cancellation for small α or fine spatial grids. A stabilized fast multipole method is presented in Section 4.2 which avoids this issue by making use of a new set of basis functions for modified biharmonic potentials. That section also contains a discussion of the quadrature-by-expansion method in the modified Stokes setting, which we use to evaluate the velocity $\mathbf{u}$ in the domain.

4.1 Background

4.1.1 Stokes equations

We begin with the steady Stokes equations, i.e. the case $\alpha = 0$, and assume zero body forces. In the stream function formulation, the velocity $\mathbf{u}$ is given

by $\mathbf{u} = \nabla^\perp \Psi$, in which case mass conservation (4.3) is automatically satisfied. Substituting this representation into the governing equations and taking the curl results in the following biharmonic equation:

$$\Delta^2 \Psi = 0 \quad \text{in } \Omega \,, \tag{4.5}$$

$$\nabla \Psi = -\mathbf{g}^\perp \quad \text{on } \Gamma \,, \tag{4.6}$$

where $\mathbf{g}^\perp = (g_2, -g_1)$. For a simply connected domain, the compatibility condition (4.4) implies that the stream function is single valued. In the case of a multiply connected domain, there does not necessarily exist a single-valued stream function Ψ without further restrictions on the boundary data $\mathbf{g}$.

There is a rich literature for integral representations of Ψ in this setting and the related setting of the Airy stress function formulation for the plane theory of elasticity. Many of the classical formulas are based on the observation of Goursat that any biharmonic function Ψ may be written in terms of two analytic functions. We have

Theorem 4.1. *(Goursat's theorem [23].) If Ψ is a biharmonic function, then there exist ϕ and ψ, analytic, such that*

$$\Psi(\mathbf{x}) = \mathrm{Re}\left(\bar{z}\phi(z) + \chi(z)\right) \,, \tag{4.7}$$

where $\chi' = \psi$ and $z = x_1 + ix_2$.

Interestingly, such a representation exists even for multiple-valued stream functions (in which case ϕ and ψ may be multiple-valued). For the Stokes equations,

the quantities of physical interest are given by $\nabla^{\perp}\Psi$. In terms of the Goursat functions, we have

Lemma 4.2. *(Muskhelishvili's formula [49].) Let* Ψ *be given as in* (4.7). *Then*

$$\frac{\partial \Psi}{\partial x_1} + i\frac{\partial \Psi}{\partial x_2} = \phi(z) + z\overline{\phi'(z)} + \overline{\psi(z)}. \tag{4.8}$$

Given (4.8), it is also clear how the velocity boundary conditions (4.6) are expressed in terms of the Goursat functions.

To obtain an integral representation for Ψ, we write the analytic functions ϕ and ψ as layer potentials. In the elasticity context, the famous Sherman-Lauricella representation leads to a second-kind Fredholm equation with a smooth kernel (for a smooth boundary), see [53] for details. In [26], the authors proposed a Sherman-Lauricella type representation for the Stokes problem in multiply-connected domains and presented some numerical results. For this representation, ϕ and ψ are not single-valued but the corresponding velocity field $\nabla^{\perp}\Psi$ is.

While the Goursat function formulation is elegant, it relies on complex analysis, and to the author's knowledge, has no generalization to the $\alpha \neq 0$ case. There is, however, a more general method for obtaining integral representations for Stokes velocity fields based on fundamental solutions of the Stokes problem. The so-called completed double layer method is based on the work of Karilla, Kim, Miranda, Power, and Pozrikidis [36, 55, 56, 57, 58]. As noted in [26], in the case of two-dimensional Stokes, the completed double layer method and the Sherman-Lauricella type approach are equivalent. We present some details of the completed double layer method for modified Stokes in the next section and the Stokes version is analogous.

Finally, we mention the thesis [21], which concerns general boundary value problems for the biharmonic equation. In brief, the integral formulations of [21] are obtained by taking linear combinations of the quadruple and octuple layer potentials of the biharmonic Green's function in a systematic fashion. The resulting integral kernels are chosen to be smooth as functions restricted to the boundary. However, because the formulations involve quadruple layer potentials, the resulting solutions (and their derivatives) can be difficult to evaluate numerically for points near (but not on) the boundary.

4.1.2 Analogues for modified Stokes

In [34], the authors followed the procedure of [21] to design an integral representation for the modified Stokes problem in terms of a stream function. Let the velocity field be given by $\mathbf{u} = \nabla^{\perp}\Psi$. Then, the stream function Ψ satisfies

$$\begin{aligned} \Delta^2\Psi - \alpha^2\Delta\Psi &= 0 \quad \text{in } \Omega\,, & (4.9)\\ \nabla\Psi &= -\mathbf{g}^{\perp} \quad \text{on } \Gamma\,. & (4.10) \end{aligned}$$

The Green's function for the modified biharmonic equation (4.9) is given by

$$G(\mathbf{x},\mathbf{y}) = -\frac{1}{2\pi\alpha^2}\left(\log\|\mathbf{x}-\mathbf{y}\| + K_0(\alpha\|\mathbf{x}-\mathbf{y}\|)\right)\,. \tag{4.11}$$

As noted in [34], the multiple-layer potentials resulting from this Green's function have the same jump properties as those of the biharmonic Green's function up to order 4. Therefore, the multiple layer potentials used in [21] for the biharmonic problem could in principle be used to represent the stream function Ψ (substituting

the Green's function for the modified biharmonic equation as appropriate). The representation of [34] set

$$\Psi(\mathbf{x}) = \int_\Gamma G_1(\mathbf{x},\mathbf{y})\sigma_1(\mathbf{y}) + G_2(\mathbf{x},\mathbf{y})\sigma_2(\mathbf{y})\, dS(\mathbf{y}) \,, \tag{4.12}$$

where

$$G_1 = -2G_{\nu\nu} + \Delta G \,, \tag{4.13}$$

$$G_2 = G_{\nu\nu\nu} + 3G_{\nu\tau\tau} - \alpha^2 G_\nu \,, \tag{4.14}$$

which, without the lower order term $-\alpha^2 G_\nu$ added to G_2, is the combination of layer potentials used in [21]. We note that G_2 is an octuple layer potential and that the velocity field $\mathbf{u}$ is given as $\nabla^\perp\Psi$. With a simple preconditioner, this representation results in a second kind integral equation for the densities σ_1 and σ_2.

In the completed double layer method, the analogues of the Laplace single layer and double layer potentials are derived to obtain integral representations for the modified Stokes equations. We follow the presentation of [58] for the Stokes equations, which begins with the derivation of Stokeslets and stresslets. The modified Stokeslet represents the velocity field induced by a point charge at $\mathbf{y}$ oriented in the direction $\boldsymbol{\sigma}$. Let $\mathbf{u}$ be such a velocity field. Then

$$-(\Delta\mathbf{u} - \alpha^2\mathbf{u}) + \nabla p = \delta(\mathbf{x}-\mathbf{y})\boldsymbol{\sigma} \,, \tag{4.15}$$

$$\nabla\cdot\mathbf{u} = 0 \,, \tag{4.16}$$

$$\mathbf{u} \;\rightarrow\; 0 \quad \text{as } \|\mathbf{x}\| \rightarrow \infty \,. \tag{4.17}$$

Letting $G_L(\mathbf{x}, \mathbf{y})$ be the Green's function for the Laplace equation in free space, we have that $\delta(\mathbf{x} - \mathbf{y}) = -\Delta G_L(\mathbf{x}, \mathbf{y})$. Making this substitution in (4.15) and taking the divergence, we find

$$\Delta p = \Delta(-\nabla G_L(\mathbf{x}, \mathbf{y}) \cdot \boldsymbol{\sigma}) \,, \tag{4.18}$$

so that

$$p = -\nabla G_L(\mathbf{x}, \mathbf{y}) \cdot \boldsymbol{\sigma} \tag{4.19}$$

Substituting this pressure into (4.15), we have

$$\begin{aligned}
(\alpha^2 - \Delta)\mathbf{u} &= 0 - \Delta G_L(\mathbf{x}, \mathbf{y})\boldsymbol{\sigma} + \nabla(\nabla G_L(\mathbf{x}, \mathbf{y}) \cdot \boldsymbol{\sigma}) && (4.20)\\
\mathbf{u} &= (-\Delta I + \nabla \otimes \nabla)(\alpha^2 - \Delta)^{-1} G_L(\mathbf{x}, \mathbf{y})\boldsymbol{\sigma} && (4.21)\\
\mathbf{u} &= (-\Delta I + \nabla \otimes \nabla) G(\mathbf{x}, \mathbf{y})\boldsymbol{\sigma} && (4.22)\\
\mathbf{u} &= (-\nabla^\perp \otimes \nabla^\perp) G(\mathbf{x}, \mathbf{y})\boldsymbol{\sigma} \,, && (4.23)\\
& && (4.24)
\end{aligned}$$

where G is the free space Green's function for the modified biharmonic equation as above. Often, the term modified Stokeslet is also used to refer to the tensor

$$\mathbf{G} = (-\nabla^\perp \otimes \nabla^\perp) G(\mathbf{x}, \mathbf{y}) \,. \tag{4.25}$$

The field induced by a continuous distribution of modified Stokeslets on a boundary

Γ, i.e.

$$\mathbf{u}(\mathbf{x}) = \mathbf{S}\boldsymbol{\sigma}(\mathbf{x}) := \int_\Gamma \mathbf{G}(\mathbf{x},\mathbf{y})\boldsymbol{\sigma}(\mathbf{y})\, dS(\mathbf{y}) \ , \tag{4.26}$$

is referred to as the single layer potential for the modified Stokes equations.

The total stress field associated with the modified Stokeslet is called a stresslet. Accordingly, the tensor $\mathbf{T}$ defined by

$$T_{ijk} = -\delta_{ik}p_j + \partial_{x_k}G_{ij} + \partial_{x_i}G_{kj} \ , \tag{4.27}$$

is also referred to as the stresslet. It is perhaps clarifying to consider the two dimensional tensor which results from applying $\mathbf{T}$ to a vector. We have

$$\begin{aligned} \mathbf{T}_{\cdot,\cdot,k}\nu_k &= -\boldsymbol{\nu}\otimes\mathbf{p} - \partial_{\nu_y}\mathbf{G} - \nabla_y(\boldsymbol{\nu}\cdot\mathbf{G}) && (4.28)\\ &= -\boldsymbol{\nu}\otimes\mathbf{p} + \nabla_y^\perp\otimes\nabla_y^\perp\left(\partial_{\nu_y}G\right) + \nabla_y\otimes\nabla_y^\perp\left(\partial_{\tau_y}G\right) \ , && (4.29)\end{aligned}$$

where $\mathbf{p}$ is the one-tensor which gives the pressure field of the Stokeslet when applied to a vector, i.e. $\mathbf{p} = -\nabla G_L$.

The double layer potential for modified Stokes is defined by

$$u_i(\mathbf{x}) = \mathbf{D}\boldsymbol{\mu}(\mathbf{x}) := \int_\Gamma T_{jik}(\mathbf{x},\mathbf{y})\nu_k(\mathbf{y})\mu_j(\mathbf{y})\, dS(\mathbf{y}) \ , \tag{4.30}$$

where $\boldsymbol{\mu}$ is a density on the curve Γ and $\boldsymbol{\nu}$ is the normal to the curve. We see that this is an integral of the adjoint of the tensor (4.29) applied to $\boldsymbol{\mu}$. In order to simplify the following expressions, we write $\boldsymbol{\mu} = \mu_\tau\boldsymbol{\tau} + \mu_\nu\boldsymbol{\nu}$, where $\boldsymbol{\tau}$ is the unit tangent to the curve. We have

$$
\begin{aligned}
\left(\mathbf{T}_{\cdot,\cdot,k}\nu_k\right)^T \boldsymbol{\mu} &= -\mathbf{p}\otimes\boldsymbol{\nu}\boldsymbol{\mu} + \nabla_y^{\perp}\otimes\nabla_y^{\perp}\left(\partial_{\nu_y} G_M\right)\boldsymbol{\mu} \\
&\quad + \nabla_y^{\perp}\otimes\nabla_y\left(\partial_{\tau_y} G\right)\boldsymbol{\mu} \qquad (4.31) \\
&= \nabla G_L \mu_\nu + 2\nabla^{\perp}\left(\partial_{\nu_y\tau_y} G\right)\mu_\nu \\
&\quad + \nabla^{\perp}\left(\partial_{\tau_y\tau_y} G - \partial_{\nu_y\nu_y} G\right)\mu_\tau \ . \qquad (4.32)
\end{aligned}
$$

We see that the velocity induced by the tangential part of the density is

$$
\nabla^{\perp}\int_{\Gamma}\left(\partial_{\tau_y\tau_y} G(\mathbf{x},\mathbf{y}) - \partial_{\nu_y\nu_y} G(\mathbf{x},\mathbf{y})\right)\mu_\tau(\mathbf{y})\ , \qquad (4.33)
$$

which is the same velocity field induced by the kernel G_1 of [34].

The jump conditions for these layer potentials are the same as in the case of the Stokes equation. We summarize them in the following theorems.

Theorem 4.3. *Let Ω, Γ, Ω_e, and Γ^* be as in Chapter 1, with Γ of class C^2. Then, the single layer potential satisfies the modified Stokes equations in Ω and Ω_e and is continuous in $\mathbb{R}^2$. Let $\mathbf{x}_0 \in \Gamma$ and $\nu_0 = \nu(\mathbf{x}_0)$. The limiting values of the surface traction $\mathbf{f}$ of the field satisfy the following jump relations*

$$
\lim_{h\to 0^+}\mathbf{f}(\mathbf{u}(\mathbf{x}_0 \mp h\nu_0)) = \pm\frac{1}{2}\boldsymbol{\sigma}(\mathbf{x}_0) + \nu(\mathbf{x}_0)_k \oint_{\Gamma} T_{ijk}\sigma_j(\mathbf{y})\, dS(\mathbf{y})\ , \qquad (4.34)
$$

where the symbol $\oint$ indicates that the integral is interpreted in the Cauchy principal value sense.

The kernel for the traction problem in the single layer formulation, i.e. the kernel in the right hand side of (4.34), is weakly singular when restricted to the

boundary. Therefore, the Fredholm alternative applies to the resulting integral equation.

For the double layer potential, we have

Theorem 4.4. *Let Ω, Γ, Ω_e, and Γ^* be as in Chapter 1, with Γ of class C^2. Then, the double layer potential satisfies the modified Stokes equations in Ω and Ω_e. Let $\mathbf{x}_0 \in \Gamma$ and $\nu_0 = \nu(\mathbf{x}_0)$. The limiting values of the field satisfy the following jump relations*

$$\lim_{h\to 0^+} \mathbf{u}(\mathbf{x}_0 \mp h\nu_0) \;=\; \mp\frac{1}{2}\boldsymbol{\mu}(\mathbf{x}_0) + \int_\Gamma T_{jik}(\mathbf{x}_0,\mathbf{y})\nu_k(\mathbf{y})\mu_j(\mathbf{y})\, dS(\mathbf{y}) \;, \quad (4.35)$$

where the symbol $\oint$ indicates that the integral is interpreted in the Cauchy principal value sense. Moreover, the traction $\mathbf{f}$ is continuous across Γ.

The kernel for the velocity problem in the double layer formulation, i.e. the kernel in the right hand side of (4.35), is weakly singular when restricted to the boundary. Therefore, the Fredholm alternative applies to the resulting integral equation.

Consider the integral equation which results from the double layer potential formulation of the velocity boundary value problem on an interior domain. We have

$$-\frac{1}{2}\boldsymbol{\mu}(\mathbf{x}_0) + \int_\Gamma T_{jik}(\mathbf{x}_0,\mathbf{y})\nu_k(\mathbf{y})\mu_j(\mathbf{y})\, dS(\mathbf{y}) = \mathbf{g}(\mathbf{x}_0) \;. \quad (4.36)$$

It is clear that for a function $\mathbf{g}$ which satisfies the compatibility condition (4.4), solutions of

$$-\frac{1}{2}\boldsymbol{\mu}(\mathbf{x}_0) + \int_\Gamma T_{jik}(\mathbf{x}_0, \mathbf{y})\nu_k(\mathbf{y})\mu_j(\mathbf{y})\, dS(\mathbf{y}) + \boldsymbol{\nu}(\mathbf{x}_0)\mathcal{W}\mu_\nu(\mathbf{x}_0) = \mathbf{g}(\mathbf{x}_0)\ , \qquad (4.37)$$

where $\mathcal{W}$ is as in Chapter 1, are also solutions of (4.36) (as the integral of μ_ν along the boundary will be zero).

To establish the existence of solutions to (4.37), we employ the Fredholm alternative. Let $\boldsymbol{\mu}$ solve the adjoint homogeneous equation

$$-\frac{1}{2}\boldsymbol{\mu}(\mathbf{x}_0) + \int_\Gamma T_{ijk}(\mathbf{x}_0, \mathbf{y})\nu_k(\mathbf{x}_0)\mu_j(\mathbf{y})\, dS(\mathbf{y}) + \boldsymbol{\nu}(\mathbf{x}_0)\mathcal{W}\mu_\nu(\mathbf{x}_0) = \mathbf{0}\ . \qquad (4.38)$$

Then, $\mathbf{u} = \mathbf{S}\boldsymbol{\mu}$ and the corresponding pressure p solve the zero traction problem in the exterior. Further, $\mathbf{u}$ tends to zero at infinity and p is bounded. This implies that $\mathbf{u} \equiv \mathbf{0}$ and that $p \equiv c_e$ for some constant in the exterior. Because $\mathbf{S}\boldsymbol{\mu}$ is continuous, this implies that $(\mathbf{u}, p)$ solves the interior problem with zero velocity conditions, so that $\mathbf{u} \equiv \mathbf{0}$ and $p \equiv c_i$ in the interior. Therefore, $\mathbf{u} \equiv \mathbf{0}$ and $\partial_{x_i}\mathbf{u} \equiv \mathbf{0}$ for $i = 1, 2$ on $\mathbb{R}^2$. Using the jump conditions for the traction of the single layer, we see that $\mu_\tau = 0$ and that $\mu_\nu = c_i - c_e$ on the boundary. Because the integral of μ_ν is zero, we see that $\mu_\nu = 0$ and therefore the solutions of (4.37) exist and are unique.

4.2 A stabilized fast multipole method

In order to evaluate the solutions to the modified Stokes problem using the double layer formulation as presented in the previous section, we'd like to use the QBX

(quadrature by expansion) method coupled with the FMM. This requires suitable multipole and local expansions, and their corresponding translation operators, for the modified biharmonic Green's function. Looking at the formula, we see that this Green's function is given as the difference of two Green's functions, those for the Laplace and modified Helmholtz equations, for which the desired results are well known. Unfortunately, applying the FMM separately to these kernels and taking the difference results in catastrophic cancellation for small values of the parameter α or on fine grids. Therefore, we develop a new approach.

4.2.1 Catastrophic cancellation for small α and fine grids

The modified biharmonic Green's function $G(\mathbf{x}, \mathbf{y})$ has a very mild singularity for $\mathbf{y}$ near $\mathbf{x}$. Indeed $G(\mathbf{x}, \mathbf{y}) = \mathcal{O}(r^2|\log r|)$, for $r = |\mathbf{x}-\mathbf{y}|$ small. For the integral equations of the previous section, we are interested in the evaluation of quadrupole and octopole moments of G, which have $\mathcal{O}(|\log r|)$ and $\mathcal{O}(1/r)$ singularities, respectively. If we were to use the fact that $G(\mathbf{x}, \mathbf{y}) = (G_L(\mathbf{x}, \mathbf{y}) - G_Y(\mathbf{x}, \mathbf{y}))/\alpha^2$, where G_L is the Laplace Green's function and G_Y the modified Helmholtz Green's function, we would take the difference of the corresponding quadrupole and octopole moments of G_L and G_Y. For these kernels, the singularities of quadrupoles and octopoles are $\mathcal{O}(1/r^2)$ and $\mathcal{O}(1/r^3)$, respectively, so that the calculation would result in catastrophic cancellation for small r (similar reasoning shows that this is also the case for small α).

We illustrate the above with a simple example. Let a collection of quadrupoles of the modified biharmonic equation be distributed as in Figure 4.1, with random weights and directions. We evaluate the total potential induced by these charges at the target points shown, which are placed in a well-separated box. The evaluation

is done in two ways: (1) the potential is evaluated using a stable method based on the asymptotics for the modified biharmonic Green's function and (2) the potential is evaluated by taking the difference of the Laplace and modified Helmholtz parts. We repeat this evaluation as we change the scale of the location of the charges and targets and as we change the modified biharmonic parameter α. The error in the second method is reported in Table 4.1. We see that we lose about two digits of accuracy for each tenfold decrease in either the scaling parameter or the modified biharmonic parameter α, as is expected. We do not report the error in the stable method, described below, which achieves machine precision in all cases.

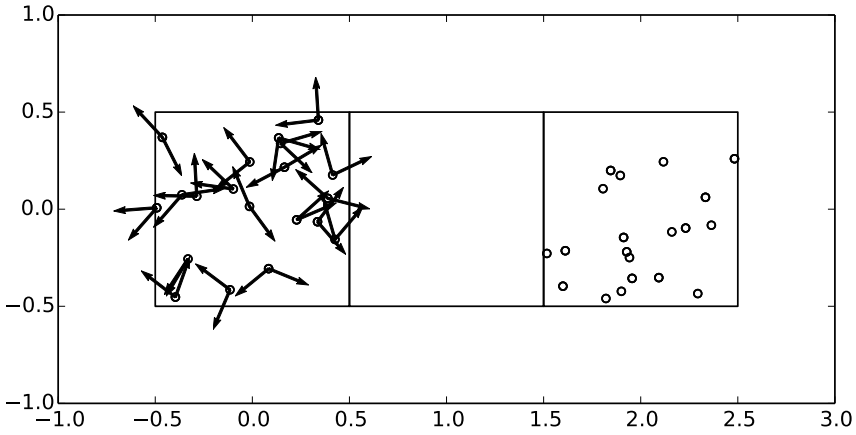

Figure 4.1: An arrangement of quadrupole charges and target evaluation points. The two vectors at each point indicate the directions of the directional derivatives.

scale	α	error	scale	α	error
1.0E0	1.0E0	1.27E-16	1.0E0	1.0E0	1.33E-16
1.0E-1	1.0E0	2.35E-15	1.0E0	1.0E-1	5.46E-15
1.0E-2	1.0E0	6.15E-13	1.0E0	1.0E-2	2.60E-13
1.0E-3	1.0E0	7.03E-11	1.0E0	1.0E-3	3.17E-11
1.0E-4	1.0E0	3.59E-09	1.0E0	1.0E-4	3.25E-09
1.0E-5	1.0E0	9.93E-07	1.0E0	1.0E-5	5.41E-07

Table 4.1: Error in using the difference of the Laplace and modified Helmholtz components to evaluate the potential due to modified biharmonic quadrupoles.

4.2.2 New basis functions

To avoid the catastrophic cancellation problem identified in the previous section, we seek out new multipole and local expansion functions for the modified biharmonic Green's function. To begin, let h be a modified biharmonic function in the exterior of a disc, given by separation of variables as

$$h(r,\theta) = \sum_{n=-\infty}^{\infty} f_n(r) e^{in\theta} \,, \tag{4.39}$$

for radial functions f_n, which are to be determined. Because the modified biharmonic operator is the composition of the Laplace and modified Helmholtz operators, we know that f_n can be written as a linear combination of $r^{-|n|}$ and $K_n(\alpha r)$ (and f_0 as a linear combination of $\log(r)$ and $K_0(\alpha r)$). Therefore, if we were to obtain new basis functions for the f_n they would be a linear combination of these. Intuitively, the issue outlined in the previous section results from the fact that the $K_n(\alpha r)$ and $r^{-|n|}$ are very similar functions for small r. They are linearly independent but have the same asymptotic behavior to leading order. We construct basis functions which do not have this property.

For small r and $n \neq 0$, the functions $K_n(\alpha r)$ have a singularity given by

$$K_n(\alpha r) = \frac{2^{|n|-1}(|n|-1)!}{\alpha^{|n|} r^{|n|}} + \mathcal{O}(|\log r| + r^{-|n|+2}) \ . \tag{4.40}$$

Let Q_n for $n \neq 0$ be defined by

$$Q_n(r) = K_n(\alpha r) - \frac{2^{|n|-1}(|n|-1)!}{\alpha^{|n|} r^{|n|}} \ , \tag{4.41}$$

so that Q_n is a linear combination of $K_n(\alpha r)$ and $r^{-|n|}$. Similarly, let Q_0 be defined by

$$Q_0(r) = K_0(\alpha r) + \log(r) \ . \tag{4.42}$$

These functions can then be evaluated stably using the appropriate asymptotics for small r. Moreover, quadrupolar sources are stably represented in this basis.

We note that the Laplace and modified Helmholtz functions for the interior of a disc, $I_n(\alpha r)$ and $r^{|n|}$, are also asymptotically similar in the way described above. For the interior of a disc, we define the functions $R_n(r)$ by

$$R_n(r) = I_n(\alpha r) - \left(\frac{\alpha r}{2}\right)^{|n|} \frac{1}{|n|!} \ . \tag{4.43}$$

It is straightforward to check that we have canceled out the first term in the power series for I_n. Moreover, the potential due to quadrupolar sources has a stable local representation in this basis.

Let the $Q_n(r)$ and $K_n(\alpha r)$ be basis functions for an outgoing representation of a modified Stokes potential h. For simplicity, we consider a real valued h which we write as $h = \mathrm{Re}(\phi)$ and the translation operators below are given for ϕ (in the style of the multipole translation operators in Chapter 1). Using the formulas

for translating Laplace and modified Helmholtz multipole expansions, we have the following formula for translating a multipole expansion in this basis.

Theorem 4.5. *Suppose that*

$$\phi(\mathbf{x}) = \sum_{l=-\infty}^{\infty} \left(a_l Q_l(\rho') + b_l K_l(\alpha\rho')\right) e^{il\theta'} \,, \tag{4.44}$$

where (ρ', θ') *are the polar coordinates of* $\mathbf{x}$ *with respect to the point* $\mathbf{x}_0$*, is a multipole expansion of the potential due to a charge density which is contained inside the disc of radius* R *about* $\mathbf{x}_0$*. Let* (ρ_0, θ_0) *be the polar coordinates of* $\mathbf{x}_0$ *with respect to the origin. Then, for* $\mathbf{x}$ *outside the disc of radius* $R + \rho_0$*, we have*

$$\phi(\mathbf{x}) = \sum_{l=-\infty}^{\infty} \left(c_l Q_l(\rho) + d_l K_l(\alpha\rho)\right) e^{il\theta} \,, \tag{4.45}$$

where (ρ, θ) *are the coordinates of* $\mathbf{x}$ *with respect to the origin. We have that* $c_0 = a_0$ *and*

$$\begin{aligned} d_0 = &\sum_{m=-\infty}^{-1} (a_m + b_m) I_{-m}(\alpha\rho_0) e^{-i(l-m)\theta_0} + a_0 R_0(\alpha\rho_0) + b_0 I_0(\alpha\rho_0) \\ &+ \sum_{m=1}^{\infty} (a_m + b_m) I_{-m}(\alpha\rho_0) e^{-i(l-m)\theta_0} \,. \end{aligned} \tag{4.46}$$

For $l > 0$ *the translated coefficients are given by*

$$c_l = \sum_{m=0}^{l} a_m \left(\frac{\alpha\rho_0}{2}\right)^{l-m} \frac{e^{-i(l-m)\theta_0}}{(l-m)!} \tag{4.47}$$

and

$$d_l = \sum_{m=-\infty}^{-1} (a_m + b_m) I_{l-m}(\alpha\rho_0) e^{-i(l-m)\theta_0} + \sum_{m=0}^{l} (a_m R_{l-m}(\rho_0) + b_m I_{l-m}(\alpha\rho_0)) e^{-i(l-m)\theta_0} + \sum_{m=l+1}^{\infty} (a_m + b_m) I_{l-m}(\alpha\rho_0) e^{-i(l-m)\theta_0} \ . \tag{4.48}$$

For $l < 0$ the translated coefficients are given by

$$c_l = \sum_{m=l}^{0} a_m \left(\frac{\alpha\rho_0}{2}\right)^{|l-m|} \frac{e^{-i(l-m)\theta_0}}{|l-m|!} \tag{4.49}$$

and

$$d_l = \sum_{m=-\infty}^{l-1} (a_m + b_m) I_{l-m}(\alpha\rho_0) e^{-i(l-m)\theta_0} + \sum_{m=l}^{0} (a_m R_{l-m}(\rho_0) + b_m I_{l-m}(\alpha\rho_0)) e^{-i(l-m)\theta_0} + \sum_{m=1}^{\infty} (a_m + b_m) I_{l-m}(\alpha\rho_0) e^{-i(l-m)\theta_0} \ . \tag{4.50}$$

We will write local expansions in terms of R_n and $(\alpha r)^{|n|}$. The following provides a formula for transforming a multipole expansion into a local expansion.

Theorem 4.6. *Suppose that*

$$\phi(\mathbf{x}) = \sum_{l=-\infty}^{\infty} \left(a_l Q_l(\rho') + b_l K_l(\alpha\rho')\right) e^{il\theta'} \ , \tag{4.51}$$

where (ρ', θ') are the polar coordinates of $\mathbf{x}$ with respect to the point $\mathbf{x}_0$, is a mul-

tipole expansion of the potential due to a charge density which is contained inside the disc of radius $R < |\mathbf{x}_0|$ about $\mathbf{x}_0$. Let (ρ_0, θ_0) be the polar coordinates of $\mathbf{x}_0$ with respect to the origin. Then, for $\mathbf{x}$ within the disc of radius $\rho_0 - R$, we have

$$\phi(\mathbf{x}) = \sum_{l=-\infty}^{\infty} \left(c_l R_l(\alpha\rho) + d_l(\alpha\rho)^{|l|} \right) e^{il\theta} \ , \tag{4.52}$$

where (ρ, θ) are the coordinates of $\mathbf{x}$ with respect to the origin. For all l, we have that

$$c_l = \sum_{m=-\infty}^{\infty} (-1)^m (a_m + b_m) K_{l-m}(\alpha\rho_0) e^{i(l-m)\theta_0} \ . \tag{4.53}$$

For $l > 0$, we have

$$\begin{aligned} d_l = \frac{1}{2^l l!} \sum_{m=-\infty}^{0} (-1)^m (a_m Q_{l-m}(\rho_0) + b_m K_{l-m}(\alpha\rho_0)) e^{-i(l-m)\theta_0} \\ + \frac{1}{2^l l!} \sum_{m=1}^{\infty} (-1)^m (a_m + b_m) K_{l-m}(\alpha\rho_0) e^{-i(l-m)\theta_0} \ . \end{aligned} \tag{4.54}$$

For $l = 0$, we have

$$d_0 = \sum_{m=-\infty}^{\infty} (-1)^m (a_m Q_{-m}(\rho_0) + b_m K_{-m}(\alpha\rho_0)) e^{im\theta_0} \tag{4.55}$$

For $l < 0$, we have

$$d_l = \frac{1}{2^{|l|} |l|!} \sum_{m=-\infty}^{-1} (-1)^m (a_m + b_m) K_{l-m}(\alpha\rho_0) e^{-i(l-m)\theta_0}$$

$$+\frac{1}{2^{|l|}|l|!}\sum_{m=0}^{\infty}(-1)^m(a_mQ_{l-m}(\rho_0)+b_mK_{l-m}(\alpha\rho_0))e^{-i(l-m)\theta_0}\ . \tag{4.56}$$

Finally, we have the following formula for translating local expansions.

Theorem 4.7. *Suppose that*

$$\Psi(\mathbf{x})=\sum_{l=-\infty}^{\infty}(a_lR_l(\rho)+b_l(\alpha\rho)^{|l|})e^{il\theta}\ , \tag{4.57}$$

where (ρ,θ) are the polar coordinates of $\mathbf{x}$ with respect to the origin, is a local expansion for a parent box centered at the origin. Let (ρ_0,θ_0) be the polar coordinates of the center $\mathbf{x}_0$ of a child box with respect to the origin. Then, for $\mathbf{x}$ inside the child box, we have

$$\Psi(\mathbf{x})=\sum_{l=-\infty}^{\infty}(c_lR_l(\rho')+d_l(\alpha\rho')^{|l|})e^{il\theta'}\ , \tag{4.58}$$

where (ρ',θ') are the coordinates of $\mathbf{x}$ with respect to the child's center $\mathbf{x}_0$. For all l, we have

$$c_l=\sum_{m=-\infty}^{\infty}a_mI_{l-m}(\alpha\rho_0)e^{-i(l-m)\theta_0}\ . \tag{4.59}$$

For $l>0$, we have

$$\begin{aligned}d_l=&\frac{1}{2^ll!}\sum_{m=-\infty}^{l-1}a_mI_{l-m}(\alpha\rho_0)e^{-i(l-m)\theta_0}\\&+\frac{1}{2^ll!}\sum_{m=l}^{\infty}a_mR_{l-m}(\alpha\rho_0)e^{-i(l-m)\theta_0}\\&+\sum_{m=l}^{\infty}\binom{m}{l}b_m\rho_0^{|l-m|}e^{-i(l-m)\theta_0}\ .\end{aligned} \tag{4.60}$$

For $l = 0$, we have

$$d_0 = \sum_{m=-\infty}^{\infty} a_m R_{-m}(\alpha\rho_0) e^{im\theta_0} + \sum_{m=-\infty}^{\infty} b_m \rho_0^{|m|} e^{im\theta_0} \ . \tag{4.61}$$

For $l < 0$, we have

$$\begin{aligned} d_l = & \frac{1}{2^{|l|}|l|!} \sum_{m=-\infty}^{l} a_m R_{l-m}(\alpha\rho_0) e^{-i(l-m)\theta_0} \\ & + \frac{1}{2^{|l|}|l|!} \sum_{m=l+1}^{\infty} a_m I_{l-m}(\alpha\rho_0) e^{-i(l-m)\theta_0} \\ & + \sum_{m=-\infty}^{l} \binom{|m|}{|l|} b_m \rho_0^{|l-m|} e^{-i(l-m)\theta_0} \ . \end{aligned} \tag{4.62}$$

4.2.3 An FMM and QBX method in the new basis

With the formulas of the previous section, we can use the FMM as in Section 1.4 to efficiently compute far field interactions for the modified biharmonic kernel. In this case, the FMM proceeds in much the standard way, except that two sets each of multipole and local coefficients must be computed for each box. The resulting FMM does not suffer from the catastrophic cancellation problem exhibited above when using the standard Laplace and modified Helmholtz multipole expansions.

Similarly, we can couple this FMM to the quadrature by expansion (QBX) method as described in Chapter 2. Because the underlying PDE is fourth-order, we must evaluate both the potential and its normal derivative at the points surrounding the expansion center. Then, a small 2×2 linear system can be solved mode-by-mode to compute the local expansion coefficients. We use such a scheme

to compute the modified Stokes example of the next chapter.

We note that because the $R_l(\alpha r)$ grow exponentially as $e^{\alpha r}$ for large α and r, we must take care for the numerical stability of the FMM. In particular, for boxes in the hierarchy such that α times the box length is large, it is best to set the coefficients for R_l to zero (these should be zero to high precision, but any non-zero parts will be amplified by a large factor). In the QBX setting, we see that we should have a fine enough boundary mesh such that if d is the distance of a QBX center to the boundary, then $d\alpha$ is reasonably small (around 1). Otherwise, the extrapolation from the QBX center will either not capture the effect of the modified Helmholtz part of the layer potential or will suffer from numerical instability. This is a problem in the modified Helmholtz setting as well because the $I_l(\alpha r)$ functions have similar asymptotic growth.

This issue for large α is due to the fact that the modified biharmonic and modified Helmholtz Green's functions are nearly degenerate in this regime (likewise, the corresponding PDEs are scaled, singularly perturbed versions of the Euler equations and the identity operator, respectively). If the modified Stokes equations are used in the Navier-Stokes setting, where a large α could result from a short time step, it seems prudent to seek out a different approach which avoids these artificial near singularities.

Chapter 5

Numerical examples

5.1 Poisson equation

For reference, the Poisson equation in a domain Ω with boundary Γ and Dirichlet boundary conditions is

$$\Delta u = f \quad \text{in } \Omega \,, \tag{5.1}$$

$$u = g \quad \text{on } \Gamma \,. \tag{5.2}$$

Using the function extension idea, as in Chapter 2, we obtain a particular solution v as

$$v(\mathbf{x}) = \int_{\Omega_B} G_L(\mathbf{x}, \mathbf{y}) f_e(\mathbf{y})\, dy \,, \tag{5.3}$$

where Ω_B is a box containing Ω and f_e is an extension of f to that box. Then, the boundary conditions are enforced by solving

$$\Delta u_h = 0 \quad \text{in } \Omega\,, \tag{5.4}$$

$$u_h = g - v \quad \text{on } \Gamma\,, \tag{5.5}$$

and setting $u = u_h + v$. The harmonic function u_h is represented by a layer potential.

To demonstrate the geometric flexibility of these solvers, we have chosen a domain Ω as shown in Figure 5.1, which is multiply connected and has regions of high curvature. We discretize the domain using $N_p = 1018$ panels, with 16 scaled Legendre nodes on each. With this number of boundary points, the error in computing f_e and the error in computing u_h does not pollute the error in the total solution below.

The interior nodes are either chosen to be on a uniform grid or chosen adaptively, so that the extended volume density f_e is resolved on each box. In particular, for the adaptive case, we require that the L_2 norm (in the continuous sense, so that it is multiplied by the area of the box) of the difference between the local approximation and f_e (whether interpreted as extended by zero or continuously) is less than some specified tolerance for each box.

The continuous extension is represented as in Chapter 2 as the sum of a double layer potential and a constant. For the harmonic boundary correction u_h, we use a combined field representation, $u_h = (D - S)\mu$, which is complete for multiply-connected domains.

Unless noted otherwise, the computations were performed on a laptop with an Intel Core i5-3317U CPU at 1.7GHz, using the gfortran compiler. The computation

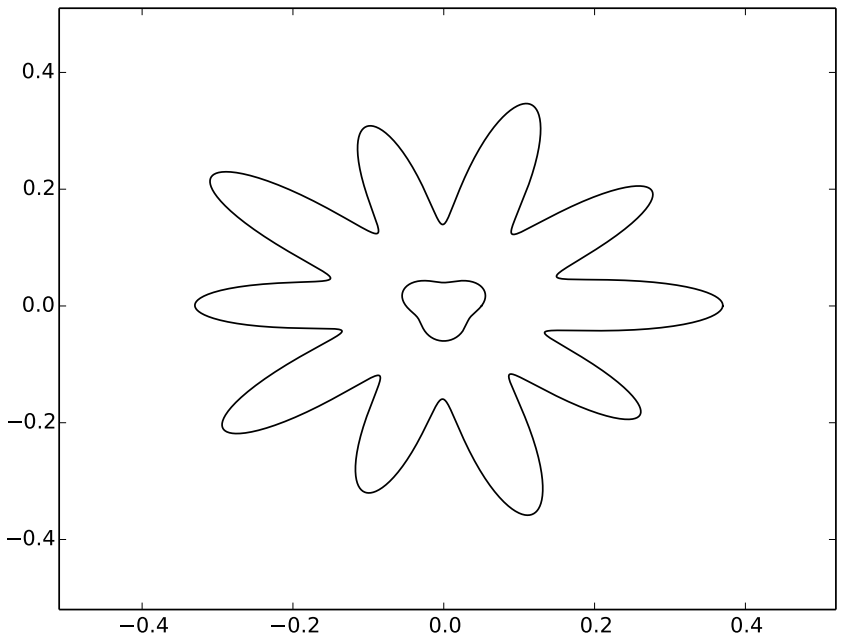

Figure 5.1: The domain Ω. The limits of the figure are those of the containing box Ω_B.

time for many of the calculations done with the boundary was flat (as the boundary was fixed). In order to solve the linear systems required for the continuous function extension and the boundary correction, we used the fast direct solver of [31]. For this domain, the precomputation step took 5.77 and 8.39 seconds for the extension and boundary correction respectively. The cost of each boundary solve was then negligible (typically .02 seconds). In many settings, the initial cost of the fast direct solver can be amortized over many different problems, e.g. if the Poisson solve is part of a larger optimization problem. To evaluate the extensions and boundary corrections throughout their respective domains, we used the quadrature by expansion method as described in Chapter 2. Forming the expansions for each expansion center required 2.4 seconds for each of these. Once the expansions were

computed, the evaluations of the potential (using the method for constant time evaluation presented in 2) consistently ran at a little over one million points per second. See Example 2 for some notes on the speed of the volume integral.

5.1.1 Example 1: continuous vs. zero extension

For Example 1, we investigate the difference in efficiency when using either continuous function extension or extension by zero. We set f and g so that the solution u is given by

$$u(\mathbf{x}) = \sin(10(x_1 + x_2)) + x_1^2 - 3x_2 + 8 \,, \tag{5.6}$$

which is fairly smooth, globally (see Figure 5.2 for a plot of the function f and its continuous extension f_e).

In Figure 5.3, we report the maximum absolute error in the computed solution as a function of the number of interior discretization nodes N for both continuous extension and extension by zero with adaptive and uniform grids. We see that the continuous extension case is much more efficient for both types of grids. For continuous extension, the adaptive grid is not more efficient until a lot of precision is requested. This is expected, as f is pretty smooth throughout the domain and continuous extension does not require that much extra refinement for boxes along the boundary (an example adaptive tree is given in Figure 5.4). In the extension by zero case, the adaptive grid is noticeably more efficient, as there is more to be gained by adding boxes near the boundary.

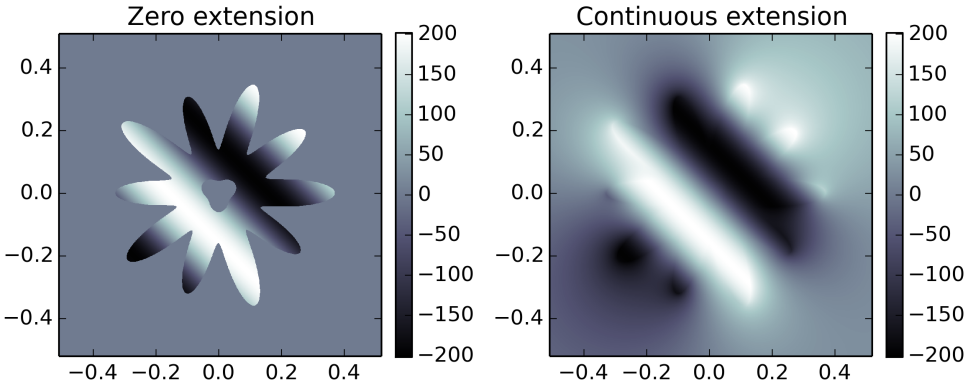

Figure 5.2: The right hand side and its continuous extension for Example 1.

5.1.2 Example 2: efficiency with adaptive grids

For the second example, we investigate the effect of using highly adaptive grids on the run time of the volume integral FMM. We set f and g so that the solution u is given by

$$u(\mathbf{x}) = \sin(10(x_1 + x_2)) + x_1^2 - 3x_2 + 8 + e^{-(500x_1)^2}\ , \tag{5.7}$$

which has a steep ridge along the x_2 axis. With this data f, the volume FMM can be much more efficient by adaptively placing many boxes near the ridge. In Figure 5.5, we show the adaptive structure that results for a given tolerance with continuous function extension, which is highly refined near the x_2 axis. It is inter-

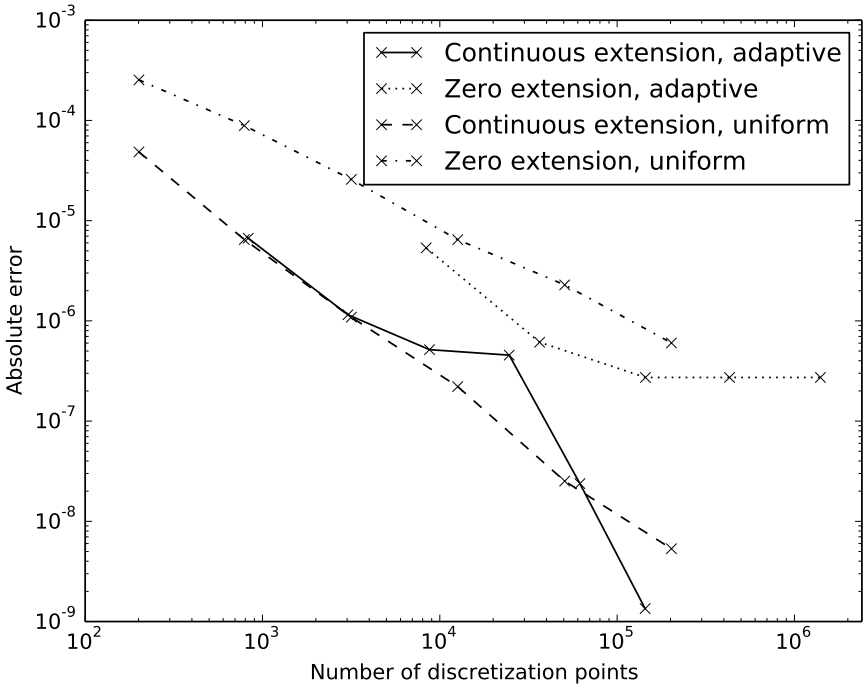

Figure 5.3: The maximum absolute error vs. the number of discretization points N in Example 1.

esting to note that because the extension is smooth outside the domain, the region of refined boxes does not extend very far beyond the boundary.

In Figure 5.6, we show the convergence rate using continuous extension for adaptive and uniform grids. The adaptive grid outperforms the uniform grid, as is expected. Remarkably, the cost of the volume FMM is essentially unaffected by using a highly adaptive grid. Let N be the number of interior degrees of freedom and N_B be the total number of degrees of freedom for the box. In Figure 5.7, we see that the total CPU time as a function of N_B is unaffected by the use of a highly adaptive grid and that the FMM runs at about one million nodes per second. The adaptive grid is capable of placing more of the degrees of freedom inside the domain itself and is therefore more efficient in terms of the CPU time

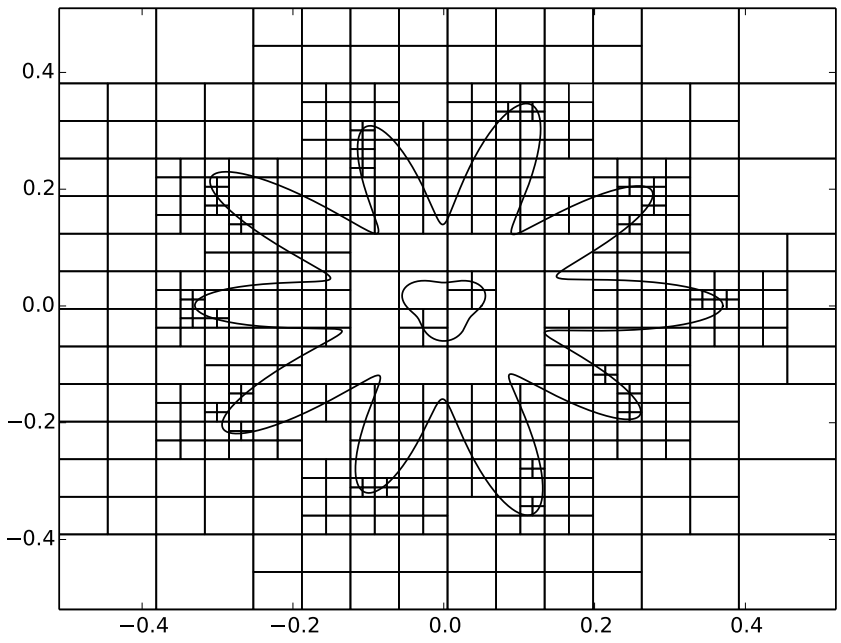

Figure 5.4: Adaptive grid using continuous extension for Example 1.

spent per interior node. For this example, we saw that the FMM with the adaptive grid ran at about half a million *interior* nodes per second.

5.2 Modified Stokes with forcing

In this section, we combine the tools of Chapters 2, 3, and 4 to solve the modified Stokes equations with a forcing term. In a domain Ω with boundary Γ, these equations are

$$\Delta \mathbf{u} - \alpha^2 \mathbf{u} = \nabla p + \mathbf{f} \quad \text{in } \Omega\,, \tag{5.8}$$

$$\mathbf{u} = \mathbf{g} \quad \text{on } \Gamma\,, \tag{5.9}$$

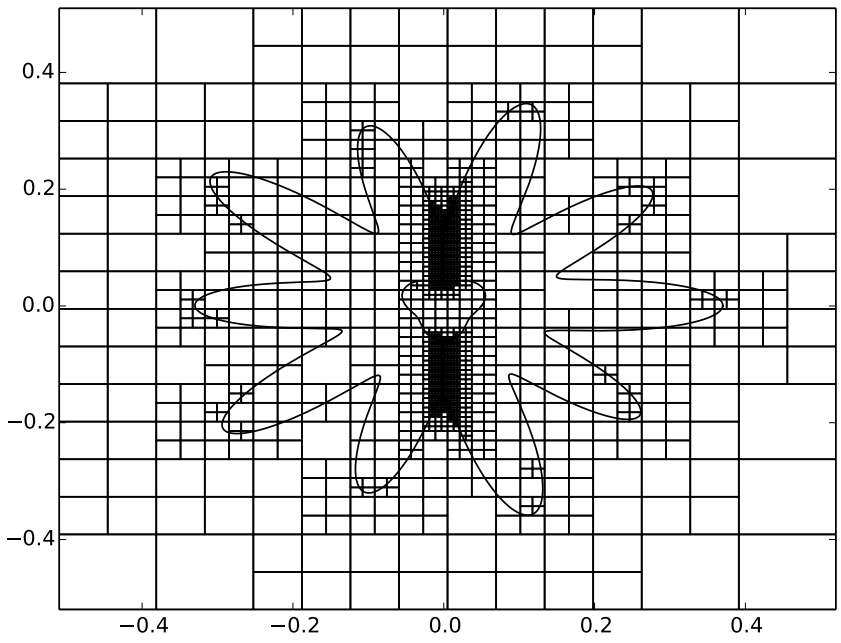

Figure 5.5: Adaptive grid using continuous extension for the anisotropic f of Example 2.

$$\nabla \cdot \mathbf{u} \;=\; 0\,. \tag{5.10}$$

As in the solution of the Poisson equation, we first compute a particular solution $\mathbf{u}_p$ which satisfies (5.8) without regard to the boundary condition. We can then compute a solution of the homogeneous modified Stokes equations, $\mathbf{u}_h$, which is equal to $\mathbf{g} - \mathbf{u}_p$ on Γ using the double layer representation for modified Stokes as presented in Chapter 4.

We assume that Ω is simply-connected, so that $\mathbf{u}_p$ may be represented using a stream function Ψ_p, without concern for the single-valuedness of Ψ_p or the corresponding pressure. Let $\mathbf{u}_p = \nabla^\perp \Psi_p$. Substituting this representation into (5.8) and taking the curl gives

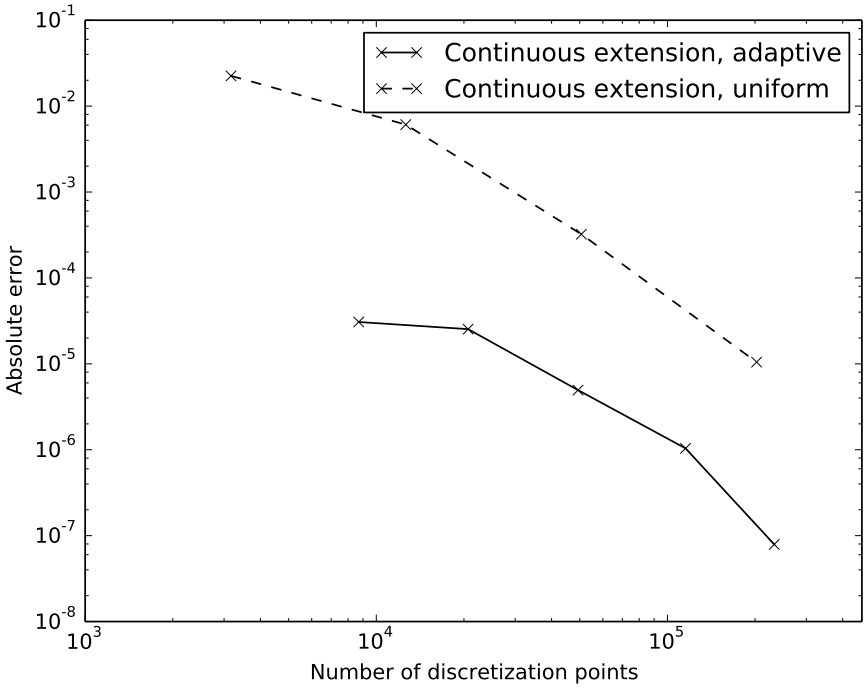

Figure 5.6: The maximum absolute error vs. the number of discretization points N in Example 2.

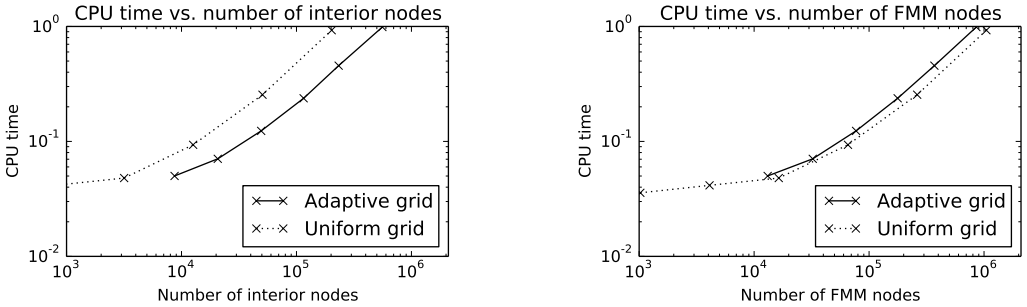

Figure 5.7: The CPU time for the volume FMM as a function of the number of interior degrees of freedom and as a function of the number of FMM nodes, for highly adaptive and uniform grids.

$$(\Delta - \alpha^2)\Delta\Psi_p = \partial_{x_2} f_1 - \partial_{x_1} f_2 \ . \tag{5.11}$$

If we let $h = \partial_{x_2} f_1 - \partial_{x_1} f_2$, then Ψ_p can be computed as the double convolution

$$\Psi_p(\mathbf{x}) = \int_{\Omega_B} G_L(\mathbf{x}, \mathbf{y}) \int_{\Omega_B} G_Y(\mathbf{y}, \mathbf{z}) h_e(\mathbf{z})\, dz\, dy \;, \tag{5.12}$$

where Ω_B is a box containing Ω and h_e is an extension of h to Ω_B. To obtain $\mathbf{u}_p$, we compute the double convolution

$$\mathbf{u}_p(\mathbf{x}) = \int_{\Omega_B} \nabla_x^{\perp} G_L(\mathbf{x}, \mathbf{y}) \int_{\Omega_B} G_Y(\mathbf{y}, \mathbf{z}) h_e(\mathbf{z})\, dz\, dy \;, \tag{5.13}$$

where the outer convolution can be obtained using the FMM as described in Section 1.4 and local derivative tables as described in [42, 4]. The first convolution can be computed using the method of Chapter 3.

To demonstrate these tools working together, we have solved the inhomogeneous modified Stokes equations with $\alpha = 1$ on the domain Ω as shown in Figure 5.8. In this case, we choose a simply-connected domain so that the particular solution may be computed as described above. We discretize the boundary using $N_p = 720$ panels, with 16 scaled Legendre nodes on each. For the calculations below, this number of discretization points ensures that the error in computing the homogeneous correction $\mathbf{u}_h$ does not pollute the error in the total solution.

For the problem to be truly inhomogeneous, we must select a force $\mathbf{f}$ which is *non-conservative*. Otherwise, the force is simply absorbed into the pressure term. We therefore choose a manufactured solution $\mathbf{u}$ given as the sum of three parts

$$\mathbf{u} = \nabla\phi + \nabla^{\perp} K + \nabla^{\perp} H \;, \tag{5.14}$$

where

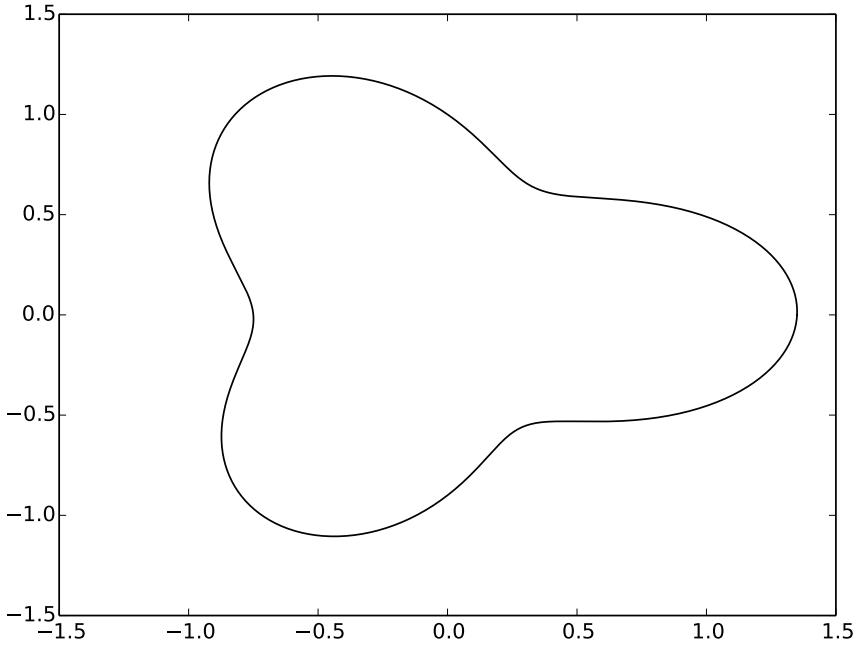

Figure 5.8: The domain Ω. The limits of the figure are those of the containing box Ω_B.

$$\phi(\mathbf{x}) = -\frac{1}{2\pi} \log |\mathbf{x} - \mathbf{x}_0| \ , \tag{5.15}$$

$$K(\mathbf{x}) = \frac{1}{2\pi} K_0(\alpha|\mathbf{x} - \mathbf{x}_0|) \ , \tag{5.16}$$

$$H(\mathbf{x}) = \frac{1}{4} Y_0(k|\mathbf{x} - \mathbf{x}_0|) \ , \tag{5.17}$$

and $\mathbf{x}_0$ is outside the domain, Y_0 is the second kind Bessel function, and $k = 20$. The corresponding $\mathbf{f}$ is non-conservative and $h = \partial_{x_2} f_1 - \partial_{x_1} f_2$ is plotted in Figure 5.9, along with its continuous extension h_e.

As this function does not require anisotropic refinement, we show results for uniform refinement of the tree, comparing zero extension and continuous extension.

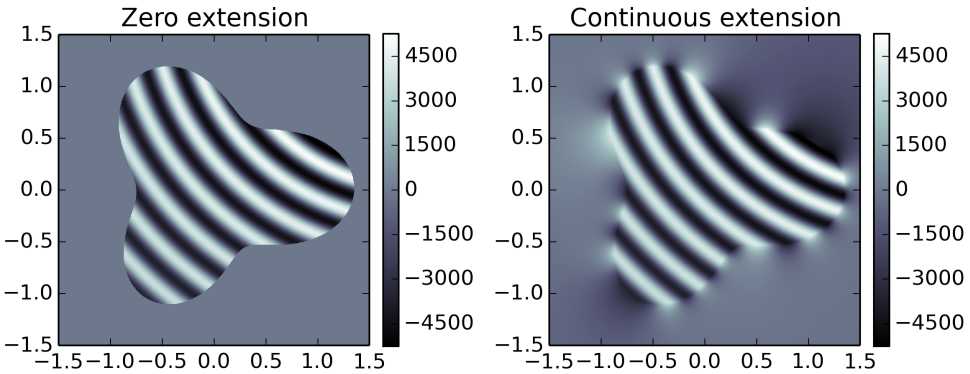

Figure 5.9: The right hand side and its continuous extension for the inhomogeneous modified Stokes example.

As in Example 1 for the Poisson equation, the adaptive scheme was actually less efficient at times than the uniform scheme because it adapted to the right hand side, rather than the solution. The results in Figure 5.10 show that the continuous extension results in a higher order convergence rate than zero extension and appears to be fourth order. This is of particular interest because it demonstrates that even the derivatives of the Laplace kernel achieve the same order of accuracy as the discretization (for a sufficiently smooth right hand side).

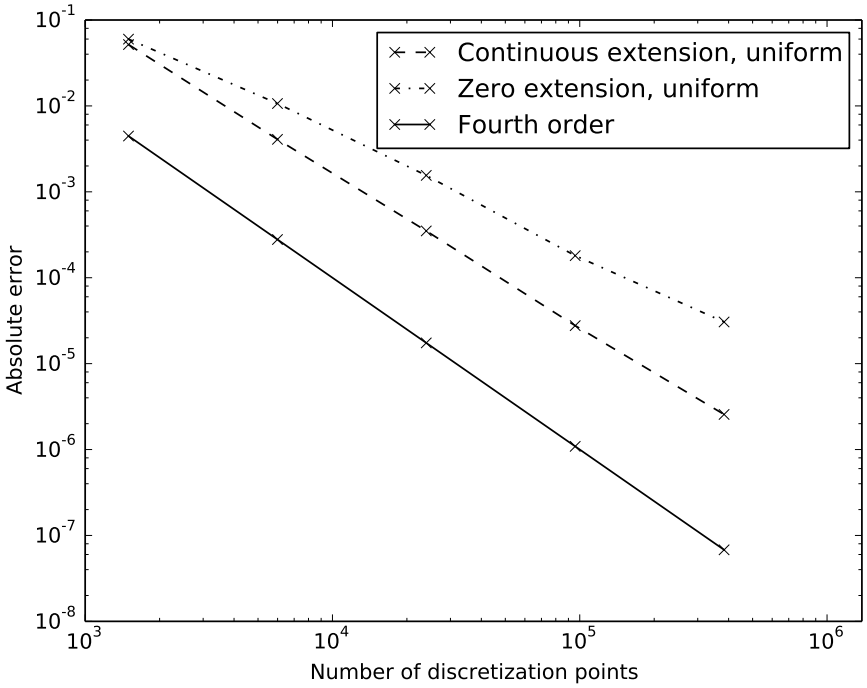

Figure 5.10: The maximum absolute error vs. the number of discretization points N in the inhomogeneous modified Stokes example. We include the line $10^4/N^2$, which represents fourth order convergence, for reference.

Chapter 6

Conclusion and future directions

In the previous chapters, we have presented a new methodology for inhomogeneous elliptic partial differential equations in complex geometry based on continuous function extension. With the tools developed therein, we have demonstrated fast solvers for the Poisson, Yukawa, and modified Stokes problems. The tools are shown to be geometrically flexible and efficient even for problems which require a lot of adaptive refinement.

There are some obvious extensions of these techniques, for instance, the ideas apply immediately to the inhomogeneous Helmholtz equation. We now discuss some possibilities for using these tools as part of the solution of more complex problems.

6.1 Variable coefficient problems

Consider the divergence-form partial differential equation

$$\nabla \cdot (\epsilon(\mathbf{x}) \nabla u(\mathbf{x})) = f(\mathbf{x}) \quad \text{in } \Omega \,, \tag{6.1}$$

$$u = g \quad \text{on } \Gamma \,, \tag{6.2}$$

where $\epsilon > 0$ is a variable coefficient. We may seek a solution u of the form

$$u(\mathbf{x}) = \int_\Omega G_L(\mathbf{x}, \mathbf{y}) \sigma(\mathbf{y}) + D\mu(\mathbf{x}) \,, \tag{6.3}$$

where G_L is the Laplace Green's function, D is the Laplace double layer potential, and σ and μ are unknown densities defined in the domain and on the boundary respectively. This results in the (well-conditioned) system of Fredholm integral equations of the second kind

$$\nabla \epsilon \cdot \left(\nabla \int_\Omega G_L(\mathbf{x}, \mathbf{y}) \sigma(\mathbf{y}) \, dy + \nabla D\mu(\mathbf{x}) \right) + \epsilon \sigma(\mathbf{x}) = f(\mathbf{x}) \quad \text{in } \Omega \,, \tag{6.4}$$

$$\int_\Omega G_L(\mathbf{x}_0, \mathbf{y}) \sigma(\mathbf{y}) \, dy + D\mu(\mathbf{x}_0) = g(\mathbf{x}_0) \quad \text{on } \Gamma \,, \tag{6.5}$$

for σ and μ. These equations may be solved iteratively and the operators on the left-hand-side may be applied using the tools of the previous chapters.

6.2 Incompressible viscous fluids

Many numerical methods for the incompressible Navier-Stokes equations require the solution of inhomogeneous elliptic equations at various points of the computation. We briefly review the underlying equations and some of the meth-

ods that are currently available. First, we write the governing equations in their standard nondimensional, primitive variables form [7, 41, 59, 61]:

$$\frac{\partial \mathbf{u}}{\partial t} + (\mathbf{u} \cdot \nabla)\mathbf{u} = -\nabla p + \frac{1}{Re}\Delta \mathbf{u} + \mathbf{f} \,, \tag{6.6}$$

$$\nabla \cdot \mathbf{u} = 0 \,. \tag{6.7}$$

For simplicity, these equations are assumed to hold in a bounded domain Ω, with $\mathbf{u}$ denoting the velocity, p denoting the pressure, Re denoting the Reynolds number, and $\mathbf{f}$ denoting a known forcing term. The vorticity is defined by $\boldsymbol{\omega} = \nabla \times \mathbf{u}$. The first equation describes a balance of viscous, inertial and pressure forces and the second (the continuity equation) enforces incompressibility. Together, they constitute a system of equations for $\mathbf{u}$ and p.

In the presence of a physical boundary, $\Gamma = \partial\Omega$, the Navier-Stokes equations must be accompanied by suitable boundary conditions, and we consider here the case where the velocity is specified:

$$\mathbf{u}|_\Gamma = \mathbf{u}_b. \tag{6.8}$$

The primitive variable formulation can be interpreted as the parabolic boundary value problem (6.6), (6.8), subject to the divergence-free constraint (6.7), for which the pressure p can be viewed as a Lagrange multiplier. A common approach to solving this system of equations is through the use of a projection method [14, 67]. In its simplest version, one first solves an approximation of the momentum equation (6.6) for one time step δt using, say, a semi-implicit backward Euler approximation:

$$\frac{\mathbf{u}^* - \mathbf{u}^n}{\delta t} - \frac{1}{Re}\Delta \mathbf{u}^* = -[(\mathbf{u} \cdot \nabla)\mathbf{u}]^n + \mathbf{f}^{n+1} \quad \text{in } \Omega \,, \tag{6.9}$$

$$\mathbf{u}^* \;=\; \mathbf{u}_b|\Gamma\ , \tag{6.10}$$

Here, $\mathbf{u}^*$ is the new estimate for the velocity and we have ignored the pressure. The second (projection) step follows by defining

$$\mathbf{u}^{n+1} = \mathbf{u}^* - \nabla p^{n+1},$$

where the pressure at the new time step p^{n+1} is chosen to enforce the continuity condition:

$$0 = \nabla \cdot \mathbf{u}^{n+1} \;=\; \nabla \cdot \mathbf{u}^* - \Delta p^{n+1} \tag{6.11}$$

$$\nabla p^{n+1} \cdot \mathbf{n} \;=\; 0|\Gamma\ . \tag{6.12}$$

Higher order versions are discussed, for example, in [8, 12]. A major advantage of the primitive variable formulation is that it is straightforward to implement using standard numerical methods for the inhomogeneous heat equation (6.9) and the Poisson equation (6.11). Indeed, using Rothe's method, the inhomogeneous heat equation may be solved with the tools presented for the modified Helmholtz problem; see, inter alia, [40, 60].

In two dimensions, one can formulate the Navier-Stokes equations entirely in terms of the scalar stream function:

$$\frac{\partial \Delta \Psi}{\partial t} + (\mathbf{u} \cdot \nabla)\Delta\Psi \;=\; \frac{1}{Re}\Delta^2\Psi + (f_2)_x - (f_1)_y\ . \tag{6.13}$$

In this formulation, the continuity equation is satisfied analytically and the boundary conditions on $(\Psi_y, -\Psi_x)$ are compatible with a fourth order partial differential

equation [25, 32, 58]. Discretization in time results in an inhomogeneous modified biharmonic equation, for which the tools of the previous chapters can be readily applied.

We believe that there are interesting opportunities for the development of new integral-equation approaches to the Navier-Stokes equations that make use of divergence-free function extension, box codes and fast homogeneous boundary-value problem solvers.

Bibliography

[1] Bradley K Alpert. Hybrid Gauss-trapezoidal quadrature rules. *SIAM Journal on Scientific Computing*, 20(5):1551–1584, 1999.

[2] Sivaram Ambikasaran and Eric Darve. An $\mathcal{O}(N \log N)$ fast direct solver for partial hierarchically semi-separable matrices: with application to radial basis function interpolation. *J. Sci. Comput.*, 57(3):477–501, 2013.

[3] Philip M Anselone and Joel Davis. *Collectively compact operator approximation theory and applications to integral equations*, volume 1971. Prentice-Hall Englewood Cliffs, 1971.

[4] Travis Askham and Antoine Cerfon. An adaptive fast multipole accelerated Poisson solver for complex geometries. Forthcoming.

[5] Kendall E. Atkinson. *The Numerical Solution of Integral Equations of the Second Kind*. Cambridge University Press, 1997. Cambridge Books Online.

[6] Alex H Barnett, Bowei Wu, and Shravan K Veerapaneni. Spectrally-accurate quadratures for evaluation of layer potentials close to the boundary for the 2D Stokes and Laplace equations. *arXiv preprint arXiv:1410.2187*, 2014.

[7] G. K. Batchelor. *An introduction to fluid dynamics*. Cambridge Mathematical Library. Cambridge University Press, Cambridge, paperback edition, 1999.

[8] John B Bell, Phillip Colella, and Harland M Glaz. A second-order projection method for the incompressible Navier-Stokes equations. *Journal of Computational Physics*, 85(2):257–283, 1989.

[9] George Biros, Lexing Ying, and Denis Zorin. The embedded boundary integral method (EBI) for the incompressible Navier-Stokes equations. Forthcoming, 2002.

[10] George Biros, Lexing Ying, and Denis Zorin. A fast solver for the Stokes equations with distributed forces in complex geometries. *Journal of Computational Physics*, 193(1):317–348, 2004.

[11] James Bremer, Zydrunas Gimbutas, and Vladimir Rokhlin. A nonlinear optimization procedure for generalized Gaussian quadratures. *SIAM Journal on Scientific Computing*, 32(4):1761–1788, 2010.

[12] David L Brown, Ricardo Cortez, and Michael L Minion. Accurate projection methods for the incompressible Navier-Stokes equations. *Journal of computational physics*, 168(2):464–499, 2001.

[13] Hongwei Cheng, Jingfang Huang, and Terry Jo Leiterman. An adaptive fast solver for the modified Helmholtz equation in two dimensions. *J. Comput. Phys.*, 211(2):616–637, 2006.

[14] Alexandre Joel Chorin. Numerical solution of the Navier-Stokes equations. *Mathematics of computation*, 22(104):745–762, 1968.

[15] Timothy A Davis. Algorithm 832: Umfpack v4. 3—an unsymmetric-pattern multifrontal method. *ACM Transactions on Mathematical Software (TOMS)*, 30(2):196–199, 2004.

[16] Timothy A Davis and Iain S Duff. An unsymmetric-pattern multifrontal method for sparse lu factorization. *SIAM Journal on Matrix Analysis and Applications*, 18(1):140–158, 1997.

[17] NIST Digital Library of Mathematical Functions. http://dlmf.nist.gov/, Release 1.0.10 of 2015-08-07. Online companion to [52].

[18] Charles L Epstein, Leslie Greengard, and Andreas Klockner. On the convergence of local expansions of layer potentials. *SIAM Journal on Numerical Analysis*, 51(5):2660–2679, 2013.

[19] Frank Ethridge and Leslie Greengard. A new fast-multipole accelerated Poisson solver in two dimensions. *SIAM J. Sci. Comput.*, 23(3):741–760, 2001.

[20] Lawrence C. Evans. *Partial differential equations*, volume 19 of *Graduate Studies in Mathematics*. American Mathematical Society, Providence, RI, second edition, 2010.

[21] Peter Farkas. *Mathematical foundations for fast methods for the biharmonic equation*. ProQuest LLC, Ann Arbor, MI, 1989. Thesis (Ph.D.)–The University of Chicago.

[22] P. R. Garabedian. *Partial differential equations*. John Wiley & Sons, Inc., New York-London-Sydney, 1964.

[23] E Goursat. Sur l'equation $\Delta\Delta u = 0$. *Bull. Soc. Math. France*, 26:236–237, 1898.

[24] Leslie Greengard. *The rapid evaluation of potential fields in particle systems*. MIT press, 1988.

[25] Leslie Greengard and Mary Catherine Kropinski. An integral equation approach to the incompressible Navier-Stokes equations in two dimensions. *SIAM Journal on Scientific Computing*, 20(1):318–336, 1998.

[26] Leslie Greengard, Mary Catherine Kropinski, and Anita Mayo. Integral equation methods for Stokes flow and isotropic elasticity in the plane. *Journal of Computational Physics*, 125(2):403–414, 1996.

[27] Leslie Greengard and Vladimir Rokhlin. A fast algorithm for particle simulations. *Journal of computational physics*, 73(2):325–348, 1987.

[28] Ronald B Guenther and John W Lee. *Partial differential equations of mathematical physics and integral equations*. Courier Corporation, 1988.

[29] Wolfgang Hackbusch. *Integral equations: theory and numerical treatment*, volume 120. Birkhäuser, 2012.

[30] Johan Helsing and Rikard Ojala. On the evaluation of layer potentials close to their sources. *Journal of Computational Physics*, 227(5):2899–2921, 2008.

[31] Kenneth L Ho and Leslie Greengard. A fast direct solver for structured linear systems by recursive skeletonization. *SIAM Journal on Scientific Computing*, 34(5):A2507–A2532, 2012.

[32] Thomas Y Hou and Brian R Wetton. Stable fourth order stream-function methods for incompressible flows with boundaries. *Journal of Computational Mathematics*, 27(4):441–458, 2009.

[33] Tomasz Hrycak and Vladimir Rokhlin. An improved fast multipole algorithm for potential fields. *SIAM Journal on Scientific Computing*, 19(6):1804–1826, 1998.

[34] Shidong Jiang, Mary Catherine A Kropinski, and Bryan D Quaife. Second kind integral equation formulation for the modified biharmonic equation and its applications. *Journal of Computational Physics*, 249:113–126, 2013.

[35] Sharad Kapur and Vladimir Rokhlin. High-order corrected trapezoidal quadrature rules for singular functions. *SIAM Journal on Numerical Analysis*, 34(4):1331–1356, 1997.

[36] Sangtae Kim and Seppo J Karrila. *Microhydrodynamics: principles and selected applications*. Butterworth-Heinemann, 1991.

[37] Andreas Klöckner, Alexander Barnett, Leslie Greengard, and Michael O'Neil. Quadrature by expansion: a new method for the evaluation of layer potentials. *J. Comput. Phys.*, 252:332–349, 2013.

[38] P Kolm and V Rokhlin. Numerical quadratures for singular and hypersingular integrals. *Computers & Mathematics with Applications*, 41(3):327–352, 2001.

[39] Rainer Kress. *Linear integral equations*, volume 82 of *Applied Mathematical Sciences*. Springer-Verlag, New York, second edition, 1999.

[40] Mary Catherine A. Kropinski and Bryan D. Quaife. Fast integral equation methods for Rothe's method applied to the isotropic heat equation. *Computers & Mathematics with Applications*, 61(9):2436 – 2446, 2011.

[41] Olga A Ladyzhenskaya and Richard A Silverman. *The mathematical theory of viscous incompressible flow*, volume 76. Gordon and Breach New York, 1969.

[42] Harper Langston, Leslie Greengard, and Denis Zorin. A free-space adaptive FMM-based PDE solver in three dimensions. *Communications in Applied Mathematics and Computational Science*, 6(1):79–122, 2011.

[43] M. Harper Langston. *An Adaptive Fast Multipole Method-Based PDE Solver in Three Dimensions*. PhD thesis, New York University, 2012.

[44] J Ma, V Rokhlin, and Stephen Wandzura. Generalized Gaussian quadrature rules for systems of arbitrary functions. *SIAM Journal on Numerical Analysis*, 33(3):971–996, 1996.

[45] Dhairya Malhotra and George Biros. A distributed memory fast multipole method for volume potentials. Forthcoming.

[46] Dhairya Malhotra, Amir Gholami, and George Biros. A volume integral equation Stokes solver for problems with variable coefficients. In *Proceedings of the International Conference for High Performance Computing, Networking, Storage and Analysis*, pages 92–102. IEEE Press, 2014.

[47] G. Mastroianni and M.G. Russo. Some new results on Lagrange interpolation for bounded variation functions. *Journal of Approximation Theory*, 162(7):1417 – 1428, 2010.

[48] Alan McKenney, Leslie Greengard, and Anita Mayo. A fast Poisson solver for complex geometries. *Journal of Computational Physics*, 118(2):348–355, 1995.

[49] Nikoloz Ivanovich Muskhelishvili. *Some basic problems of the mathematical theory of elasticity*. Springer Netherlands, 1977.

[50] Rikard Ojala. A robust and accurate solver of Laplace's equation with general boundary conditions on general domains in the plane. *Journal of Computational Mathematics*, 30(4):433–448, 2012.

[51] Rikard Ojala and Anna-Karin Tornberg. An accurate integral equation method for simulating multi-phase Stokes flow. *arXiv preprint arXiv:1404.3552*, 2014.

[52] F. W. J. Olver, D. W. Lozier, R. F. Boisvert, and C. W. Clark, editors. *NIST Handbook of Mathematical Functions*. Cambridge University Press, New York, NY, 2010. Print companion to [17].

[53] Vladimir Zalmanovich Parton and Pëtr I Perlin. *Integral equations in elasticity*. Mir Moscow, 1982.

[54] Charles S Peskin. Flow patterns around heart valves: a numerical method. *Journal of computational physics*, 10(2):252–271, 1972.

[55] Nhan Phan-Thien and Sangtae Kim. *Microstructures in elastic media*. Oxford Univ. Press, 1994.

[56] Henry Power. The completed double layer boundary integral equation method for two-dimensional Stokes flow. *IMA Journal of Applied Mathematics*, 51(2):123–145, 1993.

[57] Henry Power and Guillermo Miranda. Second kind integral equation formulation of Stokes' flows past a particle of arbitrary shape. *SIAM Journal on Applied Mathematics*, 47(4):689–698, 1987.

[58] Constantine Pozrikidis. *Boundary integral and singularity methods for linearized viscous flow*. Cambridge University Press, 1992.

[59] Constantine Pozrikidis. *Introduction to theoretical and computational fluid dynamics*. Oxford University Press, 2011.

[60] Bryan Douglas Quaife. *Fast integral equation methods for the modified Helmholtz equation*. PhD thesis, Science: Department of Mathematics, 2011.

[61] Luigi Quartapelle. *Numerical solution of the incompressible Navier-Stokes equations*, volume 113. Birkhäuser, 2013.

[62] Manas Rachh. *Integral equation methods for problems in electrostatics, elastostatics and viscous flow*. PhD thesis, New York University, 2015.

[63] Manas Rachh and Travis Askham. Integral equation formulation of the biharmonic problem with Dirichlet boundary conditions. Forthcoming.

[64] Youcef Saad and Martin H Schultz. GMRES: A generalized minimal residual algorithm for solving nonsymmetric linear systems. *SIAM Journal on scientific and statistical computing*, 7(3):856–869, 1986.

[65] Avram Sidi and Moshe Israeli. Quadrature methods for periodic singular and weakly singular Fredholm integral equations. *Journal of Scientific Computing*, 3(2):201–231, 1988.

[66] David Stein, Robert Guy, and Becca Thomases. A high-order immersed boundary method for solving fluid problems on arbitrary smooth domains. *Bulletin of the American Physical Society*, 60, 2015.

[67] Roger Temam. Sur l'approximation de la solution des équations de Navier-Stokes par la méthode des pas fractionnaires (ii). *Archive for Rational Mechanics and Analysis*, 33(5):377–385, 1969.